RESEARCH ARTICLE

Key Points:
- Existing anthropogenic NO_x inventory is consistent with aircraft and ground-based observations over Northeast United States during winter
- NO_x has a 22 hr lifetime, with half of NO_y present as NO_x, 37% as HNO_3 and pNO_3^-, and remaining 13% mostly as PAN
- Model reproduces NO_y partitioning and predicts a 42% NO_x export efficiency in winter, with a 55–45% split between wet and dry deposition

Correspondence to:
L. Jaeglé,
jaegle@uw.edu

Author Contributions:
Conceptualization: L. Jaeglé, V. Shah, J. A. Thornton, B. H. Lee, D. Fibiger, S. S. Brown, R. C. Cohen, A. J. Weinheimer, J. C. Schroder, J. L. Jimenez, R. J. Weber
Data curation: V. Shah, B. H. Lee, E. E. McDuffie, S. S. Brown, P. Veres, T. L. Sparks, P. J. Wooldridge, R. C. Cohen, T. L. Campos
Formal analysis: L. Jaeglé, V. Shah, B. H. Lee, E. E. McDuffie, D. Fibiger, S. S. Brown, P. Veres, T. L. Sparks, C. J. Ebben, P. J. Wooldridge, A. J. Weinheimer, T. L. Campos, D. D. Montzka, J. P. Digangi, J. *(continued)*

Nitrogen Oxides Emissions, Chemistry, Deposition, and Export Over the Northeast United States During the WINTER Aircraft Campaign

L. Jaeglé[1] , V. Shah[1] , J. A. Thornton[1] , F. D. Lopez-Hilfiker[1,2], B. H. Lee[1] , E. E. McDuffie[3,4,5] , D. Fibiger[3,4] , S. S. Brown[3,5] , P. Veres[3] , T. L. Sparks[6] , C. J. Ebben[6] , P. J. Wooldridge[6] , H. S. Kenagy[6] , R. C. Cohen[6] , A. J. Weinheimer[7] , T. L. Campos[7] , D. D. Montzka[7] , J. P. Digangi[8] , G. M. Wolfe[9,10] , T. Hanisco[9] , J. C. Schroder[4,5] , P. Campuzano-Jost[4,5] , D. A. Day[4,5], J. L. Jimenez[4,5] , A. P. Sullivan[11] , H. Guo[12] , and R. J. Weber[12]

[1]Department of Atmospheric Sciences, University of Washington, Seattle, WA, USA, [2]Now at Laboratory of Atmospheric Chemistry, Paul Scherrer Institute, Villigen, Switzerland, [3]Chemical Sciences Division, Earth System Research Laboratory, National Oceanic and Atmospheric Administration, Boulder, CO, USA, [4]Cooperative Institute for Research in Environmental Science, University of Colorado Boulder, Boulder, CO, USA, [5]Department of Chemistry, University of Colorado Boulder, Boulder, CO, USA, [6]Department of Chemistry, University of California, Berkeley, CA, USA, [7]Atmospheric Chemistry Observations and Modeling Laboratory, National Center for Atmospheric Research, Boulder, CO, USA, [8]NASA Langley Research Center, Hampton, VA, USA, [9]Atmospheric Chemistry and Dynamics Laboratory, NASA Goddard Space Flight Center, Greenbelt, MD, USA, [10]Joint Center for Earth Systems Technology, University of Maryland, Baltimore County, Catonsville, MD, USA, [11]Department of Atmospheric Science, Colorado State University, Fort Collins, CO, USA, [12]School of Earth and Atmospheric Sciences, Georgia Institute of Technology, Atlanta, GA, USA

Abstract We examine the distribution and fate of nitrogen oxides (NO_x) in the lower troposphere over the Northeast United States (NE US) using aircraft observations from the Wintertime INvestigation of Transport, Emissions, and Reactivity (WINTER) campaign in February–March 2015, as well as the GEOS-Chem chemical transport model and concurrent ground-based observations. We find that the National Emission Inventory from the U.S. Environmental Protection Agency is consistent with WINTER observations of total reactive nitrogen (^TNO_y) to within 10% on average, in contrast to the significant overestimate reported in past studies under warmer conditions. Updates to the dry deposition scheme and dinitrogen pentoxide (N_2O_5) reactive uptake probability, $\gamma(N_2O_5)$, result in an improved simulation of gas-phase nitric acid (HNO_3) and submicron particulate nitrate (pNO_3^-), reducing the longstanding factor of 2–3 overestimate in wintertime $HNO_3 + pNO_3^-$ to a 50% positive bias. We find a NO_x lifetime against chemical loss and deposition of 22 hr in the lower troposphere over the NE US. Chemical loss of NO_x is dominated by N_2O_5 hydrolysis (58% of loss) and reaction with OH (33%), while 7% of NO_x leads to the production of organic nitrates. Wet and dry deposition account for 55% and 45% of ^TNO_y deposition over land, respectively. We estimate that 42% of the NO_x emitted is exported from the NE US boundary layer during winter, mostly in the form of $HNO_3 + pNO_3^-$ (40%) and NO_x (38%).

Plain Language Summary Nitrogen oxides are a key family of pollutants emitted by cars, electric utilities, and industry. The fate of nitrogen oxides remains poorly understood especially during the winter season, when low sunlight leads to their persistence in the atmosphere. We analyze comprehensive aircraft observations of nitrogen oxides and their atmospheric products over the Northeast United States during winter 2015. This detailed chemical information allows to resolve a long-standing overestimate of the oxidation products of nitrogen oxides and places new constraints on their deposition to land ecosystems and export to the global atmosphere.

1. Introduction

Understanding the chemical evolution of nitrogen oxides (NO_x = NO + NO_2) anthropogenic emissions is critical to constraining their regional and global effects on oxidants, ozone (O_3) chemistry, inorganic and organic aerosol formation, and nitrogen deposition to ecosystems. As the seasons change from summer to winter in the midlatitudes, the lifetime of NO_x in the lower troposphere increases from 3 to 6 hr to more than a day because of the photochemical decrease in hydroxyl radical (OH) concentrations

C. Schroder, P. Campuzano-Jost, D. A. Day, J. L. Jimenez, A. P. Sullivan, H. Guo, R. J. Weber

Funding acquisition: L. Jaeglé, J. A. Thornton, S. S. Brown, R. C. Cohen, J. L. Jimenez, R. J. Weber
Investigation: L. Jaeglé, F. D. Lopez-Hilfiker, B. H. Lee, E. E. McDuffie, D. Fibiger, S. S. Brown, P. Veres, T. L. Sparks, C. J. Ebben, P. J. Wooldridge, R. C. Cohen, A. J. Weinheimer, T. L. Campos, D. D. Montzka, J. P. Digangi, J. C. Schroder, P. Campuzano-Jost, D. A. Day, J. L. Jimenez, A. P. Sullivan, H. Guo, R. J. Weber
Methodology: L. Jaeglé, V. Shah, B. H. Lee, E. E. McDuffie, S. S. Brown, C. J. Ebben, P. J. Wooldridge, R. C. Cohen, A. J. Weinheimer, T. L. Campos, J. P. Digangi, J. C. Schroder, P. Campuzano-Jost, D. A. Day, J. L. Jimenez, A. P. Sullivan, R. J. Weber
Resources: J. A. Thornton, S. S. Brown, R. C. Cohen, J. L. Jimenez
Supervision: L. Jaeglé
Visualization: L. Jaeglé
Writing - original draft: L. Jaeglé
Writing – review & editing: L. Jaeglé, V. Shah, J. A. Thornton, E. E. McDuffie, D. Fibiger, S. S. Brown, H. S. Kenagy, R. C. Cohen, J. C. Schroder, D. A. Day, J. L. Jimenez, A. P. Sullivan, R. J. Weber

(Martin et al., 2003). The main oxidation product of NO_x is generally nitric acid (HNO_3), but in the presence of volatile organic compounds (VOCs) significant amounts of peroxy acyl nitrates (PNs) and alkyl nitrates (ANs) can be produced. The transition from summer to winter is accompanied by a near cessation of biogenic emissions of VOCs in temperate continental regions. These much lower biogenic VOC emissions together with reduced OH lead to a decrease in the wintertime production of PNs and ANs and thus an increase in the relative importance of HNO_3 as a NO_x sink. At the same time, the pathway for HNO_3 chemical production shifts from the daytime reaction of NO_2 with OH to a more dominant role for nocturnal chemistry via dinitrogen pentoxide (N_2O_5) hydrolysis (Dentener & Crutzen, 1993; Evans & Jacob, 2005; Tie et al., 2001), which can also produce nitryl chloride ($ClNO_2$) on chloride-containing aerosols (Behnke et al., 1997; Finlayson-Pitts et al., 1989). Colder temperatures favor the partitioning of HNO_3 into particulate inorganic nitrate (pNO_3^-), a major component of submicron aerosol mass during winter.
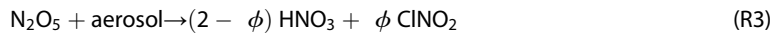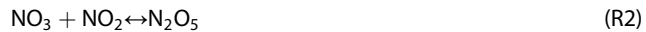
The Wintertime INvestigation of Transport, Emissions, and Reactivity (WINTER) aircraft campaign in February–March 2015 presents a unique opportunity to examine these poorly understood wintertime processes near polluted regions in the Northeast United States (NE US). Here we analyze WINTER observations of NO_x and its oxidation products (N_2O_5, HNO_3, pNO_3^-, $ClNO_2$, HONO, PNs, and ANs) with the GEOS-Chem chemical transport model (CTM). Given the paucity of field experiments during winter, we will use these aircraft observations to reexamine some challenges that have faced CTMs in past studies: constraining anthropogenic NO_x emissions, improving the representation of N_2O_5 hydrolysis, addressing the persistent bias in HNO_3 and pNO_3^- during winter, and assessing the relative importance of continental deposition versus export of NO_x and its oxidation products.

Anthropogenic NO_x emissions over the United States have been rapidly decreasing since 2000 due to emission control programs on point sources, stricter vehicle emissions standards, and changes in energy consumption driven by the economy. The U.S. Environmental Protection Agency (EPA) National Emission Inventory (NEI) reports national emissions by sector and year. The EPA estimates a 43% decrease in annual total NO_x emissions between 2005 and 2015, mostly driven by large decreases in NO_x emitted by electric utilities (−62%), industrial fuel combustion (−35%), and transportation (−47%; EPA, 2017). This decreasing trend is broadly consistent with both ground-based observations of NO_2 and satellite observations of tropospheric NO_2 columns (Duncan et al., 2016; Krotkov et al., 2016; Lamsal et al., 2015; Lu et al., 2015; Russell et al., 2012; Tong et al., 2015). For example, Krotkov et al. (2016) analyzed the 2005–2015 trends in tropospheric NO_2 columns measured by the Ozone Monitoring Instrument (OMI) onboard the Aura satellite, finding a 40% decrease over the Ohio River Valley and the I-95 megalopolis extending from Washington D.C. to New York City (DC-NYC). Similarly, Lu et al. (2015) reported a 49% decrease in OMI-derived NO_x emissions over 35 U.S. urban areas between 2005 and 2014.

Despite the broad consistency of EPA's NEI trends and observations, recent reports suggest that the magnitude of NO_x emissions from the NEI inventory, in particular motor vehicle emissions, might be overestimated by up to a factor of 2 (Anderson et al., 2014; Canty et al., 2015; Goldberg et al., 2014; Travis et al., 2016). Comparing DISCOVER-AQ aircraft observations obtained over the Baltimore/Washington region to the CMAQ model, Anderson et al. (2014) and Goldberg et al. (2014) reported a factor of 2 overestimate in NO_x, which they attribute to a combination of overestimate in mobile emissions and errors in ANs and PNs chemistry. Travis et al. (2016) used aircraft observations of NO_x and its oxidation products over the Southeast United States to infer that NEI NO_x emissions are too high by 40%, likely due to an overestimate in mobile and industrial emissions. The above studies took place during summer months in the Eastern United States, and other studies with similar conclusions took place under warm conditions in California (Brioude et al., 2013; Fujita et al., 2012; McDonald et al., 2012) and Texas (Souri et al., 2016). In contrast to these past studies, we will show that the NEI NO_x emissions inventory captures observations over the NE US during winter, pointing to potential issues with the seasonal dependence of anthropogenic NO_x emissions as represented within the NEI inventory and/or to issues with CTM's representations of boundary layer mixing and/or NO_x chemistry during summer.

During winter at midlatitudes, N_2O_5 hydrolysis on aerosols (R3) has an outsized influence on NO_x and O_3 chemistry, because of lower OH concentrations and longer nights (e.g., Alexander et al., 2009; Dentener &

Crutzen, 1993; Macintyre & Evans, 2010). At night, the following sequence of reactions lead to the formation of HNO_3:

$$NO_2 + O_3 \rightarrow NO_3 + O_2 \tag{R1}$$

$$NO_3 + NO_2 \leftrightarrow N_2O_5 \tag{R2}$$

$$N_2O_5 + \text{aerosol} \rightarrow (2 - \phi)\ HNO_3 + \phi\ ClNO_2 \tag{R3}$$

By producing $ClNO_2$ at night, (R3) can also lead to halogen activation the next morning as $ClNO_2$ photolyzes thereby influencing daytime oxidants, NO_x recycling, and O_3 production (Thornton et al., 2010). The rate of (R3) depends on aerosol surface area and on the uptake coefficient for N_2O_5, $\gamma(N_2O_5)$, which represents the probability that a N_2O_5 molecule is lost from the gas phase upon collision with a surface. Laboratory studies have demonstrated that $\gamma(N_2O_5)$ varies by several orders of magnitude depending on aerosol composition as well as phase state, temperature, and liquid water content (LWC; Abbatt et al., 2012, and references therein). Field determinations of $\gamma(N_2O_5)$ on ambient atmospheric aerosol have reported values between 2×10^{-5} and 0.175 (McDuffie et al., 2018, and references therein), with higher values on sulfate-rich aerosol and lower values for aerosol with large organic and/or nitrate content. This large variability makes model representations of $\gamma(N_2O_5)$ challenging (e.g., Davis et al., 2008; Evans & Jacob, 2000), especially as the impacts of (R3) on the concentrations of NO_x, O_3, and OH in the northern extratropics are very sensitive to $\gamma(N_2O_5)$ values between 0.001 and 0.02 (Macintyre & Evans, 2010). Laboratory experiments show that the yield for $ClNO_2$ formation, ϕ, is a strong function of particulate chloride (pCl^-) concentrations and LWC (Bertram & Thornton, 2009). Direct atmospheric observations of $ClNO_2$ demonstrate a large variability for $\phi(ClNO_2)$, spanning between 0.014 and 1 (e.g., Mielke et al., 2011; Osthoff et al., 2008; Phillips et al., 2016; Thornton et al., 2010; Wang et al., 2017). The regional impacts of $ClNO_2$ formation on the NO_x and oxidant budgets remain poorly understood as only recently have models begun to implement this reaction in their chemical mechanism (e.g., Li et al., 2016; Riedel et al., 2014; Sarwar et al., 2012, 2014).

A number of studies with the GEOS-Chem model have noted a factor of 2–3 overestimate in pNO_3^- and HNO_3 relative to surface observations over the United States during winter months (Heald et al., 2012; Walker et al., 2012; Zhang et al., 2012). This bias also exists, albeit to a somewhat smaller extent in other models and leads to a systematic overestimate of $PM_{2.5}$ concentrations over the United States and Canada during winter (Simon et al., 2012, and references therein). In an intercomparison of regional and global CTMs to surface concentrations of pNO_3^- over western Europe, Colette et al. (2011) found that four out of six models overpredicted pNO_3^- concentrations by factors of 1.5–4 during winter. The causes for this bias are unclear, but several potential explanations have been proposed: overestimate in NO_x and/or ammonia (NH_3) emissions, excessive HNO_3 production via gas phase and heterogeneous reactions, underestimate in the dry deposition velocity of HNO_3, and incorrect predictions of aerosol pH leading to incorrect HNO_3/pNO_3^- partitioning (e.g., Heald et al., 2012; Pye et al., 2018; Vasilakos et al., 2018; Zhang et al., 2012). This persistent bias calls into question the accuracy of models in predicting the response of wintertime aerosol concentrations and nitrogen deposition fluxes to reductions in anthropogenic emissions (Ellis et al., 2013; Holt et al., 2015; Lamarque et al., 2013; Pye et al., 2009; Simpson et al., 2014).

Here we use the GEOS-Chem model to show that the WINTER observations provide critical insights to these questions related to NO_x and its oxidation products. Our work complements the observationally based WINTER analyses of HNO_3/pNO_3^- partitioning by Guo et al. (2016), $\gamma(N_2O_5)$ by McDuffie et al. (2018), and of the NO_x lifetime by Kenagy et al. (2018). A number of companion papers interpret the WINTER observations with the GEOS-Chem model to examine the dominant pathways and trends in SO_4^{2-}-NO_3^--NH_4^+ aerosol formation (Shah et al., 2018); the distribution, emissions, and production of primary and secondary organic aerosol (Schroder et al., 2018); and the role of residential burning as a source of organic aerosol over the NE US (Schroder et al., 2018).

2. WINTER Aircraft Campaign and Surface Observations

The WINTER aircraft campaign took place between 1 February and 15 March 2015 out of Hampton, Virginia (https://www.eol.ucar.edu/field_projects/winter). We conducted 13 flights with the National Science
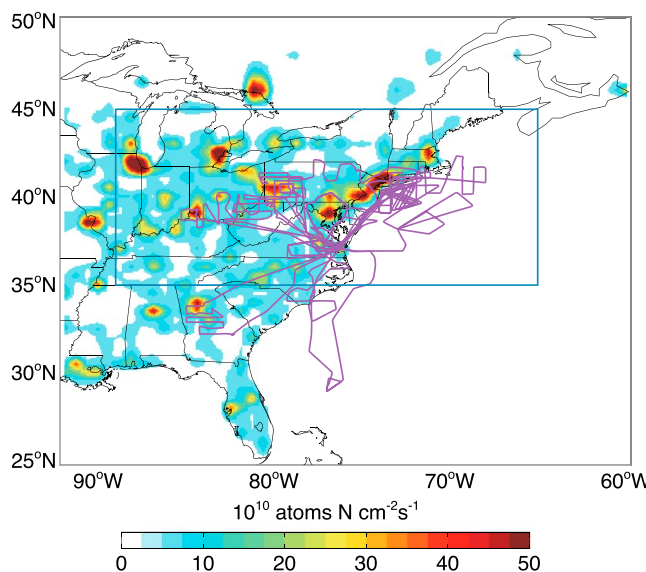
Figure 1. Surface NO_x emissions over the Eastern United States for 1 February to 15 March 2015. The WINTER NSF/NCAR C-130 flight tracks are shown in purple. The blue box delineates the Northeast United States domain, which we define as the region bounded by 35–45°N and 88.75–65°W.

Foundation/National Center for Atmospheric Research (NSF/NCAR) C-130 aircraft over the NE US (Figure 1). Flights were designed to sample the lower troposphere over and downwind of major pollution regions along the Eastern Seaboard and Ohio River Valley, with 71% of the flight hours taking place within 1 km of the surface and 85% within 2 km. As nocturnal chemistry was an important focus of WINTER, and due to the longer duration of night in winter, 58% of the flight hours were conducted at night (solar zenith angle >90°)

Table 1 summarizes the main aircraft measurements used in this study. Details on specific instruments are available in other WINTER papers (Fibiger et al., 2018; Guo et al., 2016; Lee et al., 2018; McDuffie et al., 2018; Schroder et al., 2018). Of relevance to this study, the C-130 payload included a detailed characterization not only of NO_x and total reactive nitrogen (NO_y, defined as $NO_y = NO + NO_2 + HNO_3 + HONO + 2N_2O_5 + ClNO_2 + PNs + ANs$) but also of the individual species composing NO_y. Furthermore, NO, NO_2, N_2O_5, and NO_y were each measured using two different techniques (Table 1). Duplicate measurements of the same species agreed to within 1–19% during WINTER, and the sum of individual NO_y species (ΣNO_y) was consistent with NO_y measurements to within 20–30% (Lee et al., 2018; McDuffie et al., 2018). Note that we assume that the NO_y measurements only include gas-phase reactive nitrogen species and do not sample particulate nitrate (pNO_3^-). pNO_3^- was measured separately for PM_1 (particulate matter with an aerodynamic diameter $< 1 \ \mu m$) and PM_4. Guo et al. (2016)

showed that nearly all pNO_3^- occurred as PM_1 during WINTER, and in our analysis we only use the two PM_1 pNO_3^- measurements, which agreed to within 30% (Guo et al., 2016; Schroder et al., 2018). In this paper, we will refer to ^TNO_y as the sum of NO_y and pNO_3^- ($^TNO_y = NO_y + pNO_3^-$).

Table 1
Instruments Onboard the C-130 Aircraft During WINTER Used for This Study

Variable	Time resolution[a]	Accuracy	Technique	Reference
NO_2	1 s	3%	CRDS[b]	Fuchs et al. (2009)
	1 s	10%	TD-LIF[c]	Wooldridge et al. (2010)
NO	1 s	4%	CRDS[b]	Fuchs et al. (2009)
	1 s	10%	Chemiluminescence	Weinheimer et al. (1994)
N_2O_5	1 s	12%	CRDS[b]	Dubé et al. (2006)
	1 s	30%	ToF-CIMS[d]	Lee et al. (2014, 2018)
$ClNO_2$	1 s	30%	ToF-CIMS[d]	Lee et al. (2014, 2018)
HNO_3	1 s	30%	ToF-CIMS[d]	Lee et al. (2014, 2018)
pNO_3^- (<1 μm)	1 s and 1 min	34%	HR-ToF-AMS[e]	DeCarlo et al. (2006) and Schroder et al. (2018)
	3 min	20%	PILS-IC[f]	Guo et al. (2016)
ΣPNs[g]	1 s	10%	TD-LIF[b]	Wooldridge et al. (2010)
ΣANs[g]	1 s	25%	TD-LIF[b]	Wooldridge et al. (2010)
NO_y	1 s	12%	CRDS[b]	Wild et al. (2014)
	1 s	50%	Chemiluminescence	Weinheimer et al. (1994)
HONO	1 s	50%	ToF-CIMS[b]	Lee et al. (2014, 2018)
O_3	1 s	4%	CRDS[b]	Washenfelder et al. (2011)
	1 s	5%	Chemiluminescence	Weinheimer et al. (1994)
CO	1 s	3%	UV fluorescence	Gerbig et al. (1999)
HCHO	1 s	10%	Laser-induced fluorescence	Cazorla et al. (2015)

[a]Time resolution of reported observations. For this work all observations are averaged over a 1-min time step. [b]Cavity ring-down spectrometer (CRDS). [c]Thermal dissociation laser-induced fluorescence (TD-LIF). [d]Time-of-flight chemical ionization mass spectrometer (ToF-CIMS). [e]High-resolution time-of-flight aerosol mass spectrometer (HR-ToF-AMS). [f]Particle-into-liquid sampler-ion chromatography (PILS-IC). [g]Total peroxynitrates RO_2NO_2 (ΣPNs) and total alkyl nitrates $RONO_2$ (ΣANs).

For comparison to the GEOS-Chem model, we average these observations on a uniform 1-min interval along the flight tracks. For species measured by two instruments, we take the arithmetic average of these measurements when both are available or use only the available measurement. We calculate the dry aerosol surface area by combining dry aerosol size distribution observations from the Passive Cavity Aerosol Spectrometer Probe (0.1–3 μm) and Ultra-High Sensitivity Aerosol Spectrometer (0.06–1 μm) instruments onboard the aircraft. The RH-dependent aerosol growth factors are calculated as described in McDuffie et al. (2018): for <1 μm, growth factors are derived from the High-Resolution Time-of-Flight Aerosol Mass Spectrometer (HR-ToF-AMS) observations of aerosol dry mass and estimates of aerosol liquid water; for 1- to 3-μm aerosol growth factors are calculated with the Extended-AIM Aerosol Thermodynamics Model (Wexler & Clegg, 2002) assuming pure sodium chloride particles.

We complement these aircraft observations with measurements from several surface networks in February–March 2015. We use surface observations of NO_2 and HCHO from the EPA Air Quality System (AQS) monitoring network (https://www.epa.gov/outdoor-air-quality-data). Hourly NO_2 concentrations are measured with standard chemiluminescence monitors equipped with molybdenum oxide converters (Demerjian, 2000). Daily averages of ambient HCHO concentrations are measured every 6 days using an adsorbent cartridge followed by analysis using high-performance liquid chromatography. The Clean Air Status and Trends Network (CASTNET, http://epa.gov/castnet) measures ambient concentrations of HNO_3 and $PM_{2.5}$ pNO_3^- integrated over a week. We also use measurements from the Chemical Speciation Network (CSN, https://www3.epa.gov/ttnamti1/speciepg.html) and the Interagency Monitoring of Protected Visual Environments (IMPROVE, http://vista.cira.colostate.edu/Improve/) networks, which report 24-hr mean concentrations of $PM_{2.5}$ pNO_3^- every third or sixth day. Note that the IMPROVE and CASTNET pNO_3^- measurements can be biased low due to volatilization of ammonium nitrate from the filters during sampling, storage, or shipping prior to analysis (Hand et al., 2011). Weekly wet deposition of nitrate is reported by the National Atmospheric Deposition Program/National Trends Network (NADP/NTN, https://nadp.isws.illinois.edu/). For comparison to the GEOS-Chem model, we only select sites with more than 75% temporal coverage over the 1 February to 15 March 2015 period and sample the model on the days of observations.

3. The GEOS-Chem Chemical Transport Model

3.1. General Description

We use the GEOS-Chem chemical transport model (Bey et al., 2001) driven by assimilated meteorological fields from the National Aeronautics and Space Administration GEOS-FP system (Forward Processing, Lucchesi, 2013) at 3-hr temporal resolution for 3-D fields and 1-hr resolution for 2-D fields. The original spatial resolution of GEOS-FP fields is 0.25° latitude by 0.3125° longitude and 72 vertical levels. For this study, we use a one-way nested configuration of GEOS-Chem over North America (Kim et al., 2015) with 0.5° × 0.625° resolution over North America and dynamic boundary conditions from a 4° × 5° global simulation. Initial simulations were at the native 0.25° × 0.3125° resolution, but as multiple sensitivity studies were conducted we switched to using a 0.5° × 0.625° resolution to save computational time. We found that the degraded horizontal resolution did not affect our results, confirming previous work over the Southeast United States (Yu et al., 2016). The global simulation is run for 14 months (July 2014 to March 2015) to provide initial and boundary conditions. The nested simulation is initialized on 16 January 2015 and run until 31 March 2015. Unless otherwise noted, the results presented here are for the WINTER period (1 February to 15 March 2015). For comparison to the aircraft observations, we sample the model in time and space corresponding to the location of the aircraft. We eliminate measurement time points in concentrated pollution plumes with NO_x > 10 ppbv or SO_2 > 10 ppbv, which are not resolved by the ~50 km horizontal resolution of the model. This removes 3% of the 1-min time-averaged observations.

3.2. Reference Simulation

The Reference simulation is based on the public release version 10-01 of GEOS-Chem (http://wiki.seas.harvard.edu/geos-chem/index.php/GEOS-Chem_v10-01). Boundary layer mixing uses the nonlocal scheme of Holtslag and Boville (1993) as implemented in GEOS-Chem by Lin and McElroy (2010). This scheme uses the planetary boundary layer (PBL) depth diagnosed within the GEOS-FP fields using a 2 m^2/s threshold on the total eddy diffusion coefficient of heat. During WINTER, the GEOS-FP daytime (10 a.m. to 4 p.m. local

time) mean PBL depth along the flight tracks was 830 ± 360 m over land and 1,150 ± 340 m over the ocean. We compare the monthly mean daytime maximum PBL depth observed at the Micropulse Lidar Network site in Greenbelt, Maryland, for 2001–2008 (Lewis et al., 2013) with the GEOS-FP PBL depth at that location for 2013–2016 (Figure S1 in the supporting information), finding good agreement between observed (February 1,380 ± 210 m; March 1,700 ± 160 m) and modeled (February 1,370 ± 240 m; March 1,520 ± 310 m) PBL depth. In addition, the GEOS-Chem model reproduces the vertical profiles of trace gases and aerosols observed during WINTER (section 4.1), a further indication that the PBL depth and associated mixing are simulated reasonably well during February and March.

The HO_x-NO_x-VOC-O_3-BrO_x tropospheric chemistry chemical mechanism is described in Mao et al. (2010, 2013) with recent updates for biogenic VOC chemistry (Fisher et al., 2016; Travis et al., 2016). We use $\gamma(N_2O_5)$ from Evans and Jacob (2005), which assumes aerosol-specific parameterizations for sulfate-nitrate-ammonium (SNA: SO_4^{2-}-NO_3^--NH_4^+), organic aerosol (OA), black carbon, dust, and sea salt. The aerosol multicomponent system for SNA, OA, black carbon, dust, and sea salt was most recently described in Kim et al. (2015). To simulate secondary OA, we use the SIMPLE parameterization of Hodzic and Jimenez (2011), which has been shown to perform well during WINTER (Schroder et al., 2018). The particle pH dependent gas-particle partitioning of HNO_3 and NH_3 is computed with the ISORROPIA II thermodynamic module (Fountoukis & Nenes, 2007), as implemented by Pye et al. (2009). We assume bulk metastable equilibrium of the gas phase with liquid SO_4^{2-}-NO_3^--NH_4^+ PM_1 aerosol. The public release version of GEOS-Chem includes Na^+ and Cl^- from submicron sea salt in the gas-aerosol equilibrium. In our Reference simulation, we assume that submicron sea salt is externally mixed, such that Na^+ and Cl^- ions do not participate in the HNO_3 and NH_3 gas-particle partitioning as discussed in Guo et al. (2016) and Shah et al. (2018). In addition to the aqueous phase oxidation of sulfur dioxide (SO_2) via hydrogen peroxide (H_2O_2) and O_3, included in the public release version of GEOS-Chem, we have added metal-catalyzed SO_2 oxidation following Alexander et al. (2009) as described in Shah et al. (2018).

Anthropogenic emissions over the United States are from the 2011 EPA National Emissions Inventory (NEI11v6.1) at a horizontal resolution of 0.1° × 0.1°, as implemented in GEOS-Chem by Travis et al. (2016). These emissions are adjusted to 2015 using the EPA's national annual trend report (EPA, 2017), with scaling factors of 0.8 for NO_x, 0.72 for SO_2, 0.83 for carbon monoxide (CO), and 0.93 for VOCs. The emissions are hourly and date specific. We shift the daily NEI emissions by 2 days such that the days of the week match in 2015 and 2011. As surface temperatures in February 2015 were 6 °C colder compared to the 2001 temperatures used in Gilliland et al. (2006), we adjusted hourly NH_3 emissions from livestock to 2015 temperatures following Aneja et al. (2000). This temperature adjustment resulted in a factor of 2 reduction in livestock NH_3 emissions for the WINTER period and improved agreement with WINTER observations of NH_4^+ and pNO_3^- (Shah et al., 2018). Based on tall tower and aircraft measurements, Hu et al. (2015) found that the NEI emission inventory overestimated toluene emissions by a factor of 2.5. In our Reference simulation, we reduce the NEI toluene emissions by this factor, leading to a significant reduction in the GEOS-Chem overestimate in toluene compared to WINTER aircraft observations, with a 50% overestimate instead of a factor of 3 overestimate prior to the adjustment (not shown). For shipping emissions, we replace the NEI emission inventory with the International Comprehensive Ocean- Atmosphere Data Set (Lee et al., 2011; Wang et al., 2008). The emissions are distributed based on reported monthly ship locations and are released at the surface. Shipping emissions of NO_x are processed by the PARANOX module (Vinken et al., 2011; Holmes et al., 2014) to account for O_3 and HNO_3 production in the plume. Open biomass burning emissions (wildfires and agricultural fires) are from the year-specific Global Fire Emissions Database v4 (van der Werf et al., 2017) and biogenic emissions from the Model of Emissions of Gases and Aerosols from Nature v2.1 (Guenther et al., 2012).

Wet deposition includes the processes of rainout and washout of gases and aerosols based on Liu et al. (2001) with updates from Wang et al. (2011) and Amos et al. (2012). Croft et al. (2016) found that cloud water content of precipitating clouds in GEOS-Chem's wet deposition scheme is an order of magnitude higher than observations in cold regions, which affects rainout scavenging. To address this, we modify the wet deposition scheme as described in Shah et al. (2018), by assuming a linearly decreasing value of cloud water content from 1 g/m^3 for liquid clouds ($T \geq 268$ K) to a minimum of 0.1 g/m^3 for ice clouds ($T \leq 258$ K). This modification increases wet deposition fluxes by about 20% during the winter period.
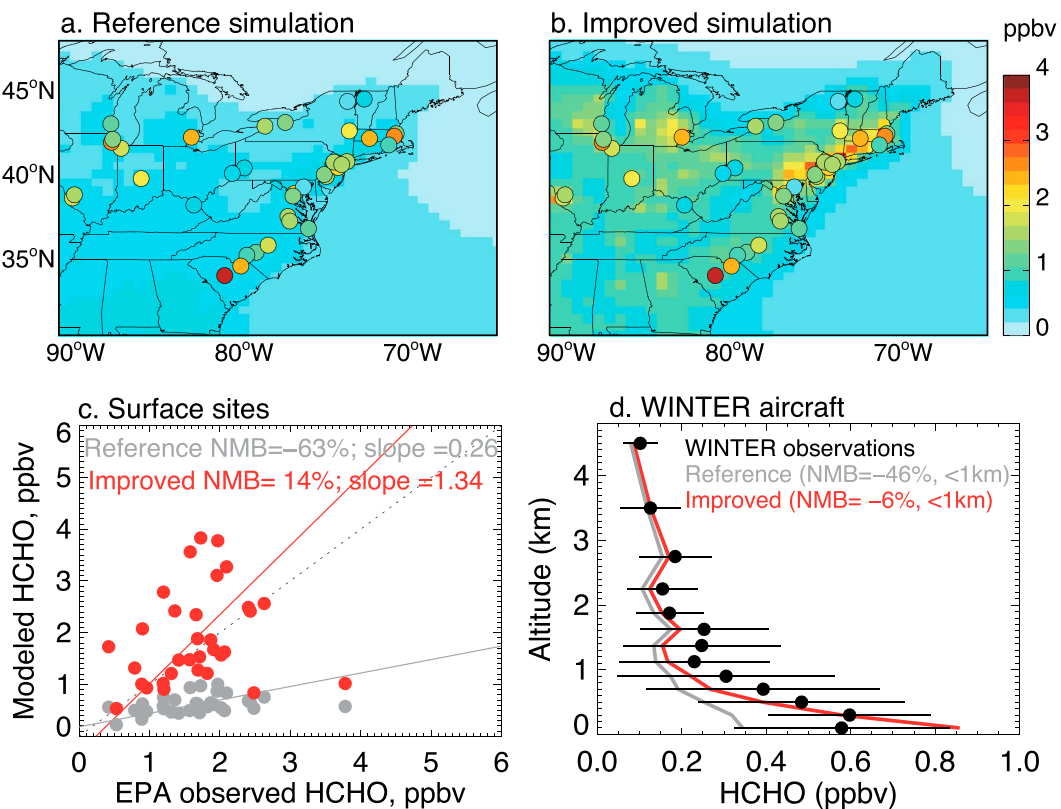
Figure 2. Comparison between observed and modeled HCHO. Top panels: Mean surface mixing ratio of HCHO for 1 February to 31 March 2015 calculated with the (a) Reference and (b) Improved GEOS-Chem simulations. The color-filled symbols show surface observations from the EPA for the same period. (c) Scatter plot between modeled and observed HCHO. The model is sampled at the location of the observations and on the days when observations are collected. Dark gray shows the Reference model and red show the Improved model. The solid lines indicate the reduced-major-axis regression lines. The Normalized Mean Bias (NMB) and slope are given on the insert. (d) Vertical profile of observed and modeled HCHO during the WINTER campaign. The filled circles and error bars are the means and standard deviations of the observations. The NMB corresponds to observations below 1 km altitude. EPA = Environmental Protection Agency.

3.3. Updates to GEOS-Chem for this Study: Improved Simulation

In addition to the reference GEOS-Chem simulation described in section 3.2, we conduct a second simulation, referred to as *Improved* simulation, with the following modifications (summarized in Table S1).

3.3.1. Wintertime Sources of HCHO

Formaldehyde (HCHO) is a key indicator of photochemistry as it is an intermediate in VOC oxidation, provides a source of HO_x radicals, and thus affects both O_3 and NO_x photochemistry. Photolysis of HCHO can be a dominant source of HO_x radicals during midlatitude winters, when low H_2O and high SZA lead to weak OH production from $O(^1D) + H_2O$ (e.g., Snow et al., 2003). Comparisons of the mean observed HCHO vertical profile during WINTER and the reference GEOS-Chem simulation show a systematic model underestimate in the boundary layer (Figure 2d). Below 1 km altitude, the Reference simulation has a -46% normalized mean bias (NMB = $100 \times \Sigma(M_i-O_i)/\Sigma O_i$, with observations O_i and model M_i summed along the flight tracks). In addition, the Reference simulation underestimates EPA surface observations of HCHO by a factor of 2.5, with a NMB of -63% (Figures 2a and 2c). Zhu et al. (2017) report a similar model bias during winter months in their evaluation of GEOS-Chem against 9 years of EPA HCHO surface observations. Luecken et al. (2012) show that CMAQ has a -69% bias compared to EPA HCHO observations for January 2002. The state-of-the-art WINTER aircraft HCHO measurements confirm the model bias found in these previous studies and demonstrate that the high HCHO concentrations are present throughout the lower troposphere. This persistent bias is unlikely due to an overestimate in HCHO sinks, which are dominated by photolysis. Thus, the systematic model underestimate

of HCHO points to missing primary emissions and/or secondary photochemical production of HCHO during winter.

In the Reference simulation over the NE US lower troposphere (defined as 35–45°N; 88.75–65°W; 0–1.7 km, blue box in Figure 1) we find that over this entire domain primary emissions of HCHO account for 10% of the HCHO source, with the remaining 90% due to secondary production, which is dominated by methane (CH_4) oxidation. In the NEI inventory the two dominant sources of HCHO over the NE US during winter are mobile emissions and residential wood combustion (RWC), accounting for 47% and 42% of primary emissions, respectively. Point sources account for 9.3% of HCHO emissions, and less than 2% are from other sources such as solvent use and waste disposal. Based on cold-start exhaust measurements of the HCHO-to-toluene emission ratio from cars at different temperatures, Jobson and Huangfu (2016) and Jobson et al. (2017) have suggested that wintertime cold temperature vehicle start emissions are underestimated by a factor of 5 in the NEI inventory. Furthermore, VanderSchelden et al. (2017) found that RWC accounted for 73% of the HCHO observed over Yakima, Washington, during winter, a much larger fraction than expected based on the NEI inventory.

To examine whether a potential underestimate in RWC and mobile emissions could explain the observed HCHO, we increase the NEI HCHO emissions for these two sources by a factor of 5 in the Improved simulation (resulting in a factor of 4.6 increase in total primary emissions of HCHO). As shown in Figure 2, the resulting HCHO in the Improved simulation is in better agreement with both aircraft and surface observations (NMB = +14% for surface observations; NMB = −6% for aircraft observations below 1 km). In this simulation, primary emissions account for 30% of the HCHO source, with 70% due to secondary production. Overall, this leads to a 20% increase in OH over the NE US in the Improved simulation.

Observed WINTER concentrations of C3 alkenes, which can be an important secondary source of HCHO, are overestimated in GEOS-Chem by 50–100% (not shown), so they cannot explain the missing HCHO. Another possible explanation to reconcile model and observations would be the rapid oxidation of larger VOCs, which are not represented in GEOS-Chem. A more in-depth analysis of whether the missing wintertime sources of HCHO are primary or secondary will be presented in a forthcoming study. For the purpose of this paper, we make the simplifying assumption that all missing HCHO is due to an underestimate of primary emissions, which we increase to match the observed HCHO mixing ratios during WINTER.

3.3.2. Simple ClNO$_2$ Chemistry

We add ClNO$_2$ as a new chemical species in the chemical mechanism. We include a simplified treatment of its chemistry, assuming that its only production is via (R3) and its only loss is via photolysis, neglecting ClNO$_2$ deposition, which is expected to be small (Kim et al., 2014). We use ClNO$_2$ cross sections from Ghosh et al. (2012). Upon photolysis of ClNO$_2$, NO$_2$ and Cl are produced. We do not track the Cl radical as chlorine chemistry is not included in this version of the model. The main concern herein is the impact of ClNO$_2$ as a NO$_x$ reservoir, which is captured by this approach. The impact of ClNO$_2$ on the oxidant budget will be examined in a separate study, in which we consider the reactions of Cl radicals with CH$_4$ and VOCs.

3.3.3. Heterogeneous Chemistry

The Evans and Jacob (2005) γ(N$_2$O$_5$) parameterization was found to overpredict direct observations of γ(N$_2$O$_5$) on ambient aerosols (Bertram et al., 2009), as well as γ(N$_2$O$_5$) derived from in situ observations of NO$_3$ and N$_2$O$_5$ (Brown et al., 2009). For SNA aerosol, we replace the Evans and Jacob (2005) γ(N$_2$O$_5$) parameterization with the Bertram and Thornton (2009) parameterization, which considers the competing effects of pNO$_3^-$, pCl$^-$, and LWC. The LWC is calculated within ISORROPIA II based on SNA aerosol composition, relative humidity, and temperature. As the version of GEOS-Chem we are using does not include full chlorine chemistry, we make the simplifying assumption that 10% of pCl$^-$ from submicron sea salt is displaced onto SNA aerosol. This is likely an underestimate of pCl$^-$ present during WINTER, as we neglect anthropogenic sources, which accounted for up to half the HCl observed during WINTER. We calculate the ClNO$_2$ yield, ϕ(ClNO$_2$), on SNA aerosol using the Bertram and Thornton (2009) parameterization as a function of LWC and pCl$^-$ concentrations. For all other aerosol we assume ϕ(ClNO$_2$) = 0, except for sea salt aerosol for which we assume ϕ(ClNO$_2$) = 1.

Evans and Jacob (2005) parameterized γ(N$_2$O$_5$) on OA using the laboratory measurements of Thornton et al. (2003) on malonic acid. However, malonic acid represents very hygroscopic organic aerosol, which accounts for a small fraction of OA in the atmosphere. Field measurements indicate that humic-like substances are
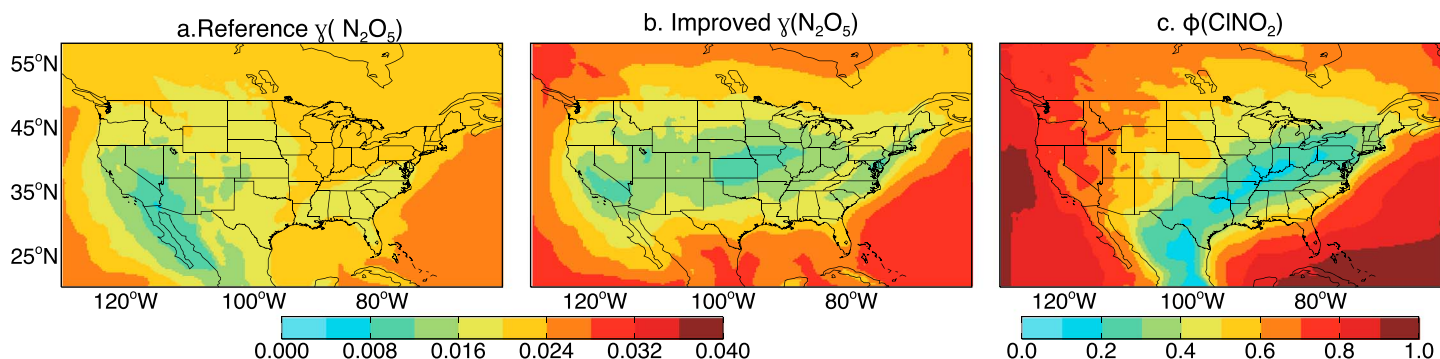
Figure 3. Spatial distribution of $\gamma(N_2O_5)$ and $\phi(ClNO_2)$ at 0.6 km altitude (950 hPa) averaged over 1 February to 15 March 2015. (a) $\gamma(N_2O_5)$ in the Reference simulation. (b) $\gamma(N_2O_5)$ in the Improved simulation with the Bertram and Thornton (2009) parameterization on SNA aerosols as a function of LWC, pNO_3^-, and pCl^- and the RH dependent $\gamma(N_2O_5)$ on OA from Badger et al. (2006). (c) $\phi(ClNO_2)$ in the Improved simulation. LWC = liquid water content; SNA = sulfate-nitrate-ammonium; OA = organic aerosol.

more representative of the broader composition of water-soluble organic compounds in the atmosphere (e.g., Fuzzi et al., 2001; Zhang et al., 2007). We thus update $\gamma(N_2O_5)$ on OA to use the laboratory measurements of Badger et al. (2006) on humic acid, with $\gamma(N_2O_5) = 10^{-4}$ for RH < 50% and 10^{-3} for RH ≥ 50%. This choice is also supported by $\gamma(N_2O_5)$ measured on mixed organic-inorganic aerosol systems (Gaston et al., 2014). These values are 1–2 orders of magnitude lower than what was previously assumed in GEOS-Chem for the OA component. For all other aerosol, we keep the same formulation as in Evans and Jacob (2005). The resulting $\gamma(N_2O_5)$ calculated at 0.6 km altitude during the WINTER campaign is shown in Figure 3b. The large pNO_3^- concentrations over the Midwest and NE US lead to a decrease in $\gamma(N_2O_5)$ from 0.02 (Reference simulation, Figure 3a) to 0.01 (Improved simulation). In coastal areas of the Eastern United States, the pCl^- dependence of $\gamma(N_2O_5)$ on SNA aerosol results in a strong $\gamma(N_2O_5)$ gradient from 0.01 to 0.03. McDuffie et al. (2018) conducted an iterative box modeling analysis fit to 10-s averages of WINTER observations of NO_2, O_3, N_2O_5, and $ClNO_2$ to infer 2,876 individual determinations of $\gamma(N_2O_5)$ from all WINTER night (SZA > 90°) flights. They found a median value of $\gamma(N_2O_5) = 0.0143$, consistent with our median Improved simulation value of 0.011. McDuffie et al. (2018) also found a strong gradient in $\gamma(N_2O_5)$ over coastal areas of the NE US (see their Figure 3b). We calculate that $\phi(ClNO_2)$ is lowest (0.1–0.3) in the continental Eastern United States with low RH and pCl^- concentrations, increasing rapidly to 0.5–0.8 over the ocean off the U.S. East Coast (Figure 3c).

Laboratory studies have reported values of $\gamma(NO_3)$ between 1.5×10^{-4} and 0.72, depending on aerosol type, with most of the values in the 10^{-4}–10^{-3} range for water with dissolved ions and for OA (e.g., Brown & Stutz, 2012, and references therein). Some of the high values measured correspond to fast initial uptake on the surface of the aerosol, after which $\gamma(NO_3)$ decays to a steady state value 1–2 orders of magnitude lower (e.g., Mak et al., 2007). The original $\gamma(NO_3)$ value assumed in GEOS-Chem was 10^{-3} based on the recommendation of Jacob (2000). Mao et al. (2013) increased $\gamma(NO_3)$ to 0.1 on all aerosol in GEOS-Chem. We decrease it back to 10^{-3}, to be consistent with the laboratory measurements summarized in Brown and Stutz (2012).

In the reference GEOS-Chem model, the products of NO_2 heterogeneous uptake on aerosol are assumed to be ½ HNO_3 + ½ $HONO$ ($\gamma(NO_2) = 10^{-4}$), based on the recommendation of Jacob (2000). As summarized in the recent review by Sparato and Ianniello (2014), laboratory studies of the heterogeneous uptake of NO_2 show that the kinetics of this reaction are first order in NO_2 and that the main observed gas-phase product is nitrous acid (HONO), with some formation of adsorbed HNO_3. However, the detailed reaction mechanisms for heterogeneous NO_2 hydrolysis remain debated and some of the adsorbed HNO_3 could be released back as NO_2 or NO (Finlayson-Pitts et al., 2003; Gustafsson et al., 2009; Jenkin et al., 1988; Ramazan et al., 2004). Furthermore, several studies show that this reaction could be photoenhanced on various aerosol surfaces, producing mainly HONO (e.g., Spataro & Ianniello, 2014, and references therein). In the Improved simulation, we assume that HONO is the only product of NO_2 heterogeneous uptake ($NO_2 \rightarrow HONO$) and keep $\gamma(NO_2) = 10^{-4}$.

3.3.4. Dry Deposition

Dry deposition velocities, v_d, are simulated in GEOS-Chem using the resistance-in-series scheme of Wesely (1989) as implemented by Wang et al. (1998). The total resistance to dry deposition (which is the inverse of v_d) is calculated as the sum of the aerodynamic resistance, R_a, the quasi-laminar boundary layer resistance, R_b, and the surface resistance, R_c. R_c includes the influence of leafs, lower canopy, and ground. Based on early observations of increasing R_c for SO_2, NO_2, and HNO_3 on snow surfaces below 0 °C (Johansson & Granat, 1986; Valdez et al., 1987), Wesely (1989) added a temperature dependent function, $1000 \exp(-T_s - 4)$ (in units of seconds per meter, with surface temperature, T_s, in degrees Celsius) to all surface resistance terms. This results in unrealistically low v_d values for $T_s < -2$ °C, in particular near-zero values for $v_d(HNO_3)$. Following more recent parameterizations, we limit the increase in R_c at low temperatures to no more than a factor of 2 (Erisman et al., 1994; Zhang et al., 2003). Furthermore, as HNO_3 has a high affinity for all natural surfaces, a common assumption is that its surface resistance is negligible (Hertel et al., 2012; Seinfeld & Pandis, 2006; Wesely & Hicks, 2000). Accordingly, we update GEOS-Chem to impose $R_c (HNO_3) = 1$ s/cm.

Over much of the NE US during the campaign, T_s ranged between 0 °C and −15 °C. Our updates increase v_d by 10–50% for most species, with a particularly large increase for $v_d(HNO_3)$ from mean values of 0.6 to 2.1 cm/s. These updated values are consistent with measurements of $v_d(HNO_3)$ reported in the literature (e.g., Janson & Granat, 1999; Pryor et al., 2002; Sievering et al., 2001), with little seasonal difference between summer and winter at sites with cold wintertime temperatures (Munger et al., 1996; Zimmermann et al., 2006).

4. Results

4.1. Vertical Distribution of Trace Gases and Aerosols During WINTER

Figure 4 displays the WINTER campaign mean observed profiles of O_3, CO, and aerosol surface area, as well as profiles of ^TNO_y ($^TNO_y = NO_y + pNO_3^-$), NO_x ($NO_x = NO+NO_2$), HNO_3, pNO_3^-, and ΣPNs. We also show nighttime vertical profiles of N_2O_5, $ClNO_2$, and HONO. Background O_3 in the free troposphere is ~50 ppbv, decreasing to ~40 ppbv near the surface where high NO_x emissions lead to net O_3 loss. The GEOS-Chem model captures this gradient and is generally within 2–5 ppbv of observations at all altitudes. The mixing ratios of O_3 increase by 2 ppbv on average in the Improved simulation relative to the Reference simulation, due to the decrease in $\gamma(N_2O_5)$ and in the associated O_3 loss via (R1)–(R3). The GEOS-Chem model underestimates CO observations throughout the troposphere by 10–20 ppbv. This appears to be related to an underestimate of background CO in the free troposphere. Such a low bias in Northern Hemisphere middle and high latitudes is a common feature in many CTMs (Monks et al., 2015; Naik et al., 2013; Shindell et al., 2006) and could indicate an overestimate of global OH concentrations in models (Strode et al., 2015, and references therein).

The model simulation reproduces the vertical profile of median aerosol surface area (Figure 4). Shah et al. (2018) provide a detailed evaluation of aerosol composition simulated in GEOS-Chem against both WINTER aircraft and ground-based observations. They find that the model reproduces the observed concentrations of SO_4^{2-}, NO_3^-, NH_4^+, and OA particulates to within 15–20%. Shah et al. (2018) showed that the median PM_1 pH calculated by GEOS-Chem along the WINTER flight tracks below 1 km altitude over land was 1.29, in good agreement with the pH of 1.34 inferred from thermodynamic analysis of observed PM_1 composition (Guo et al., 2016). This consistency between modeled and observed aerosol surface area, composition (affecting $\gamma(N_2O_5)$), and particle pH is particularly important to our estimates of NO_x loss via N_2O_5 hydrolysis, as well as to the gas/aerosol partitioning of HNO_3 which is a strong function of particulate pH (Guo et al., 2016; Shah et al., 2018).

There is a remarkable agreement between observed and modeled profiles of ^TNO_y, with mean values of 5 ppbv near the surface decreasing to less than 1 ppbv above 2 km altitude (Figure 4). The model also reproduces the vertical distribution of NO_x, HNO_3, pNO_3^-, and ΣPNs, with the Improved simulation being within 20–40% of observations. Relative to the Reference simulation, the Improved simulation results in closer agreement with observed HNO_3 and pNO_3^-, because of our updated $\gamma(N_2O_5)$ and $v_d (HNO_3)$ (section 3.3). Furthermore, the Improved simulation predicts higher concentrations of ΣPNs (taken as the sum of peroxyacetyl nitrate, peroxymethacroyl nitrate, and peroxypropionyl nitrate in GEOS-Chem), in better agreement
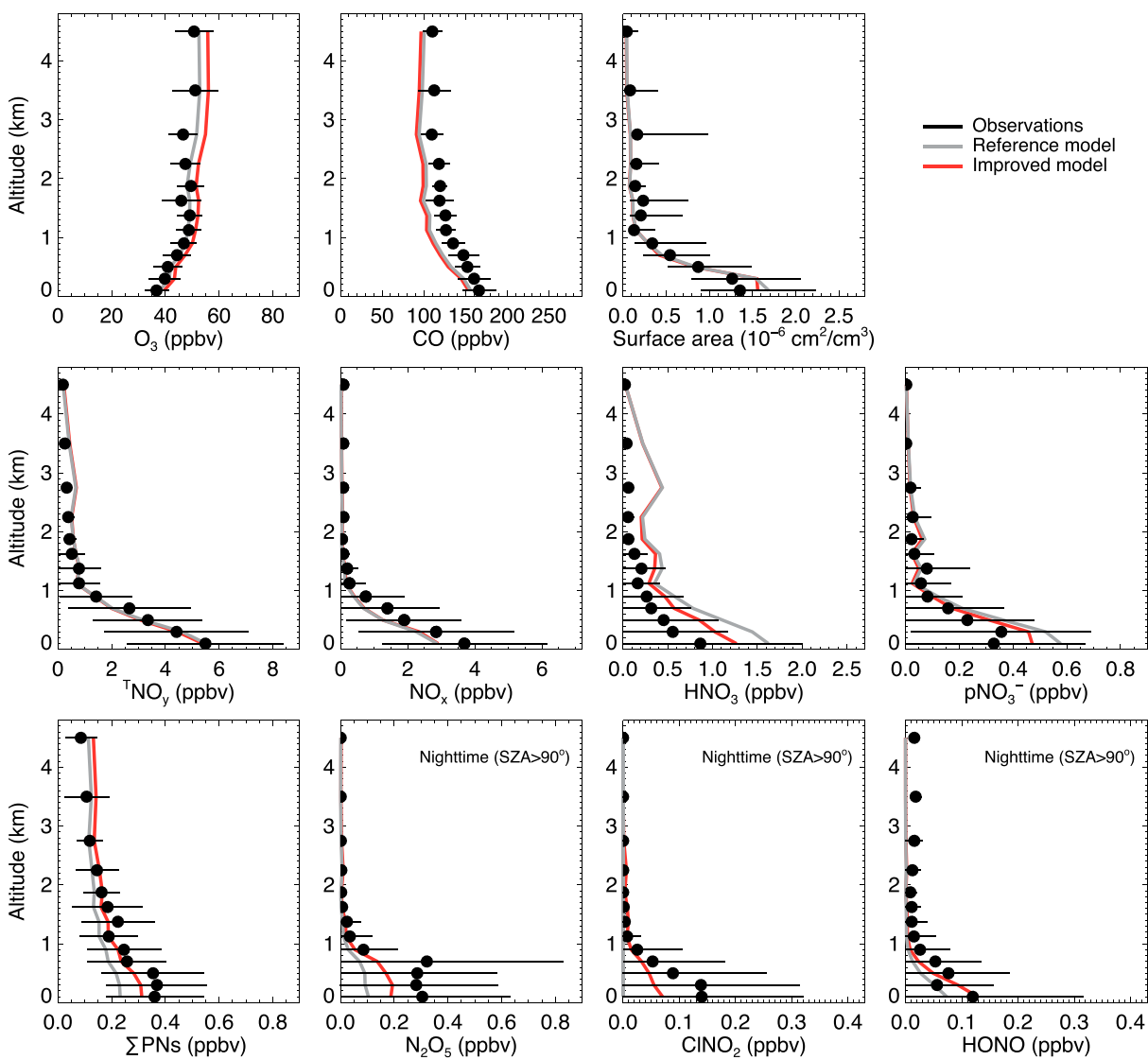
Figure 4. Mean vertical profiles of O_3, CO, aerosol surface area, $^T NO_y$ (=NO_y + pNO_3^-), NO_x, HNO_3, pNO_3^-, ΣPNs, N_2O_5, $ClNO_2$, and HONO observed (filled circles with error bars indicating the standard deviation) during WINTER and simulated with GEOS-Chem (gray lines for the reference simulation, red lines for the improved simulation). We show only nighttime (defined as SZA > 90°) profiles for N_2O_5, $ClNO_2$, and HONO. For the aerosol surface area profiles, we display the median profiles and quartiles instead of the means and standard deviations.

with observations. This is mostly due to higher HCHO concentrations (section 3.3.1), leading to more OH, enhanced RO, and RO_2 production from VOC oxidation and thus enhanced PNs production in the Improved simulation compared to the Reference simulation.

Because of the lower $\gamma(N_2O_5)$ and $\gamma(NO_3)$ assumed in the Improved simulation, GEOS-Chem predicts a doubling of nighttime N_2O_5 mixing ratios from mean values of ~100 to ~200 pptv below 1 km altitude (Figure 4). While in better agreement with observations (mean of ~300 pptv), the Improved simulation is 30–40% too low. The Improved simulation qualitatively reproduces the observed $ClNO_2$ profile but tends to underestimate observations below 500 m, which were mostly taken over water. This suggests that $\phi(ClNO_2)$ is underestimated in our simulation as discussed in more detail in section 4.3.

WINTER observations show highly variable HONO mixing ratios with mean values of 59 ± 115 pptv at night and 24 ± 45 pptv during the day (<1 km altitude). The Improved simulation predicts mean HONO of 59 ± 90 pptv at night and 16 ± 37 pptv during the day. These values are nearly a factor of 2 higher than those predicted in the Reference simulation (Figure 4), as a result of the combined effects of changing NO_2
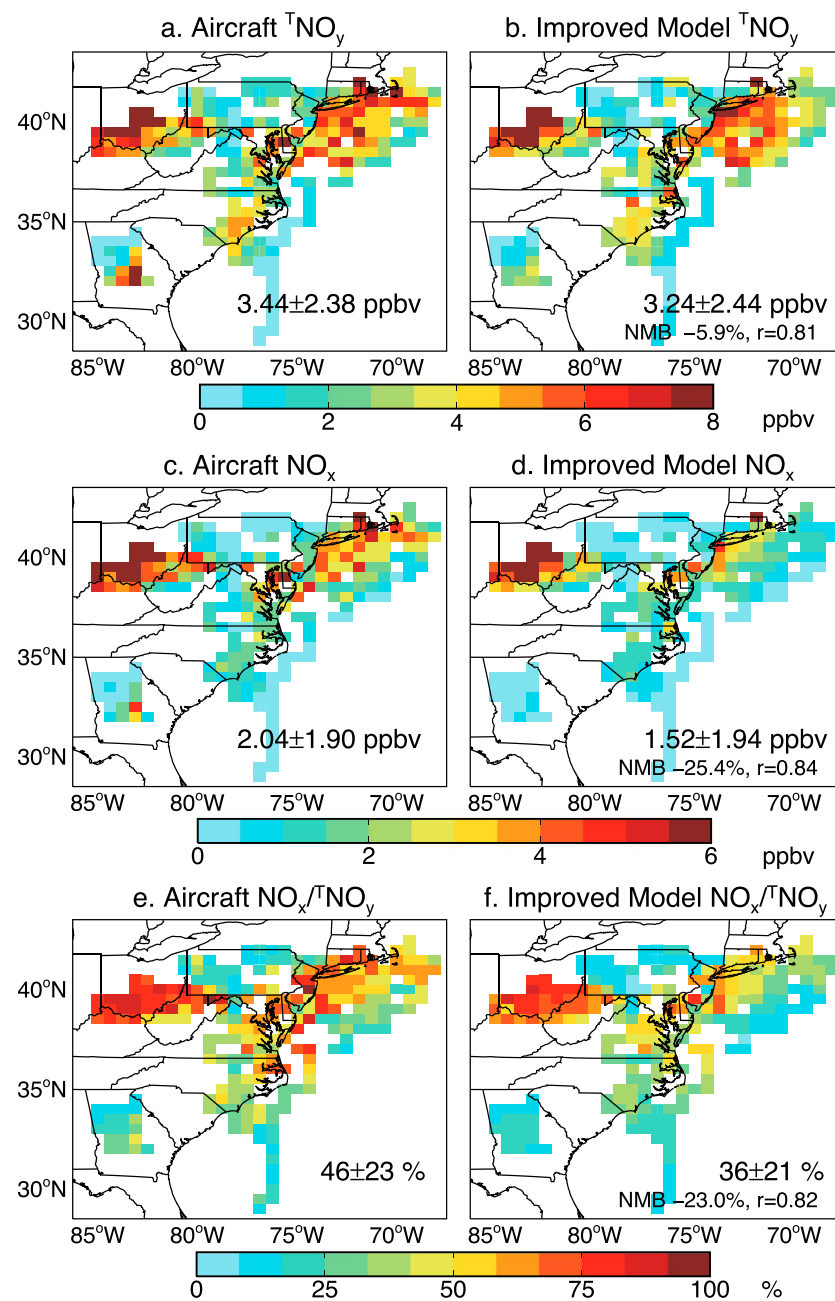
Figure 5. Spatial distribution of ^TNO_y ($NO_y + pNO_3^-$, a, b), NO_x (c, d) and $NO_x/^TNO_y$ (e, f) observed during the WINTER campaign and simulated with Improved GEOS-Chem for altitudes within 1 km of the ground. The observations are averaged over the model grid, and the model is sampled at the time and location of the aircraft. The mean and standard deviations of the mixing ratios are shown in the insert. NMB = normalized mean bias.

heterogeneous uptake to produce only HONO (section 3.3.3) and enhanced HCHO primary emissions, which increase OH and the gas-phase HONO production via NO + OH.

In the next two sections, we examine in more detail the spatial distribution of NO_x and its oxidation products.

4.2. Anthropogenic NO_x Emissions During Winter

Figures 5a and 5b show that the magnitude and spatial distribution of observed ^TNO_y below 1 km altitude is reproduced by GEOS-Chem, with the highest ^TNO_y mixing ratios (>6 ppbv) concentrated over the Ohio River
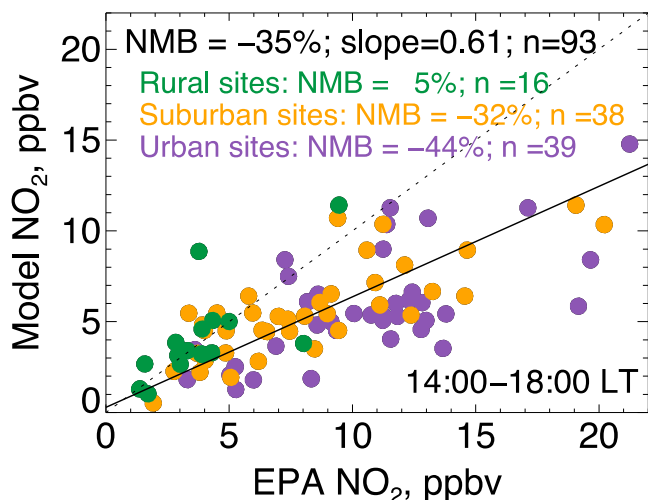
Figure 6. Comparison between modeled and observed NO_2 at EPA AQS surface sites in the NE US for 1 February to 15 March 2015 at 14:00–18:00 local time. The Improved GEOS-Chem simulation is sampled at the location of the observations and on the days when observations are collected. There are 93 sites with more than 75% daily coverage of observations for this time period. The NMB and slope are shown in the insert. We also indicate the NMB for the 16 rural sites (green), the 38 suburban sites (orange), and 39 urban sites (purple). EPA = Environmental Protection Agency; AQS = Air Quality System; NMB = normalized mean bias.

Valley and downwind of the DC-NYC megalopolis. The model displays a small negative bias (−6%) and high correlation coefficient ($r = 0.81$). Simulations with the FLEXPART particle dispersion model indicate that the WINTER campaign sampled air that was influenced by emissions 6–24 hr back. Because of the short time between emissions and sampling and the long lifetime of NO_x during winter, most of ^TNO_y is in the form of NO_x over the NE US. The observed $NO_x/^TNO_y$ ratio varies from ~70% to 90% over source regions with the highest NO_x, decreasing to 20–25% off the coast. The model reproduces this general pattern (Figures 5e and 5f). The simulated NO_x mixing ratios display a −25% bias relative to the aircraft observations below 1 km altitude. We hypothesize that this underestimate is due to a small overestimate of the NO_x oxidation rate and to an underestimate in $\phi(ClNO_2)$ (see section 4.3).

We also compare the Improved GEOS-Chem simulation to surface hourly NO_2 measurements from the EPA AQS monitoring network obtained at 93 sites in the Eastern United States between 1 February and 15 March 2015 (Figure 6). Most of these sites are in urban (39 sites) and suburban (38 sites) environments and display very strong diurnal variations with the highest NO_2 concentrations observed during the early morning rush hour, when the shallow PBL traps pollutants near the surface. As the spatial heterogeneity of NO_2 near localized sources is not resolved by the ~50 km horizontal resolution of GEOS-Chem, we focus on NO_2 observations in the afternoon (14:00–18:00 hr local time), when the PBL is deepest and mixing will lead to more homogeneity. The commercial instruments used to measure NO_2 have known interferences to NO_x oxidation products, in particular ANs, PAN, and HNO_3 (e.g., Dunlea et al., 2007; Steinbacher et al., 2007). We correct for these interferences by applying the correction factor developed by Lamsal et al. (2008), using the GEOS-Chem hourly NO_2 and its oxidation products for each site. This correction is minimal for winter months (<10%). We find that GEOS-Chem underestimates afternoon AQS NO_2 observations by 35%, slightly larger than the underestimate we found relative to aircraft NO_x observations. Restricting our comparison to rural EPA sites, the model bias is lower (NMB = +5%, Figure 6).

Overall, our comparison between the GEOS-Chem simulation and WINTER observations of ^TNO_y suggests that NO_x emissions in the NEI inventory over the NE US are consistent with aircraft observations in the bottom 1 km of the atmosphere to within 10% on average. Salmon et al. (2018) find a similar agreement between the 2011 NEI NO_x emission inventory and top-down NO_x emissions from airborne mass balance experiments conducted around the Washington D.C.-Baltimore region during WINTER. These findings are in contrast with previous studies suggesting that NEI NO_x emissions, in particular motor vehicle emissions, might be overestimated by a factor of 2 (section 1). These previous studies were focused on summer months in the Eastern United States or under warm conditions in California and Texas.

These diverging findings suggest potential issues with the seasonal dependence of anthropogenic NO_x emissions as represented within the NEI inventory. These issues could be linked to assumptions about the summer/winter vehicle fleet composition and their associated NO_x emissions. Another possibility is that models have seasonal biases in PBL mixing and/or chemistry. For example, Travis et al. (2016) found that during summertime over the SE United States GEOS-Chem systematically overestimates surface O_3 concentrations and predicts a flat vertical profile of O_3 within 1 km of the surface, while ozonesonde observations indicate a 7 ppbv increase. They attributed some of the model bias to excessive vertical mixing in the model and net surface O_3 production in the model, while observations would indicate net O_3 loss at the surface. In their evaluation of the CMAQ model, Appel et al. (2017) found that EPA surface observations showed larger NO_2 mixing ratios during winter compared to summer, especially in the early morning, while the CMAQ model predicted the opposite seasonal variation. Henderson et al. (2017)
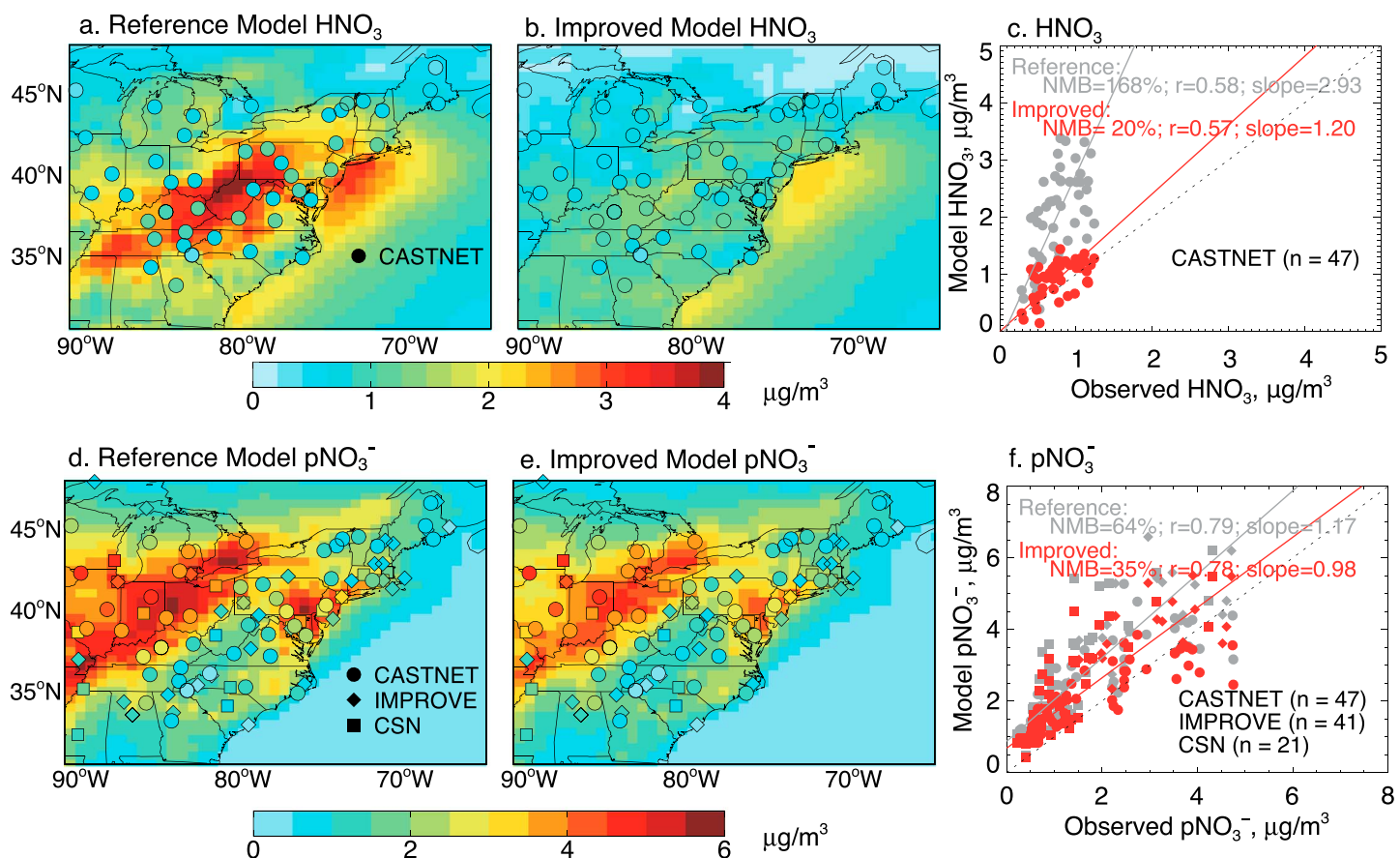
Figure 7. Surface concentrations of HNO$_3$ (a–c) and pNO$_3^-$ (d–f) measured at CASTNET, IMPROVE, and CSN sites and simulated with GEOS-Chem for 1 February to 15 March 2015. The spatial distribution of surface observations (colored symbols) is compared to the Reference (a, d) and to the Improved (b, e) GEOS-Chem simulations. The right panels show scatter plots of simulated versus observed values at individual sites. Correlation coefficients (*r*), normalized mean biases (NMB), and the slopes of the reduced major axis regression lines are listed for the Reference (gray) and Improved (red) simulations. The reduced major axis regression line (solid lines) and the 1:1 lines (dashed line) are also shown.

proposed that this discrepancy could be explained by a CMAQ underestimate in vertical mixing during summer morning hours.

In the case of WINTER observations, we reproduce the vertical profile of ^{T}NO$_y$ and other surface pollutants, giving us confidence in the representation of vertical mixing. Similarly, the chemistry of NO$_x$ and its oxidation products appears to be well represented based on the detailed constraints provided by the WINTER aircraft observations.

In their airborne mass balance study, Salmon et al. (2018) report a factor of 2 overestimate in the NEI 2011 CO emissions over the Washington D.C.-Baltimore region, which combined with the good agreement in NO$_x$ results in a factor of 2 underestimate in the CO/NO$_x$ enhancement ratio. For the WINTER observations below 0.8 km altitude we calculate a mean CO/NO$_x$ enhancement ratio of 5.4 ± 1.2 ppbv/ppbv (based on the correlation between background-subtracted CO and ^{T}NO$_y$ for daytime flights over land), similar to the 4.6 ± 0.7 and 5.1 ± 1.5 ppbv/ppbv values reported by Salmon et al. (2018). This is also in agreement with the 4.6 to 5.2 ppbv/ppbv ratios measured by Wallace et al. (2012) during winter in Boise, Idaho, near busy roads. In contrast, the NEI 2011 CO/NO$_x$ emission ratio is 8.7 ppbv/ppbv for the NE US and the GEOS-Chem CO/^{T}NO$_y$ enhancement ratio sampled along the C-130 flight tracks 10.1 ± 0.6 ppbv/ppbv. Thus, we find that the NEI inventory overestimates CO emissions by factors of 1.6–1.9 over the NE US. This was not initially apparent in the vertical profile in Figure 4 because of the free tropospheric CO underestimate. The CO/NO$_x$ ratios reported by summertime studies are generally
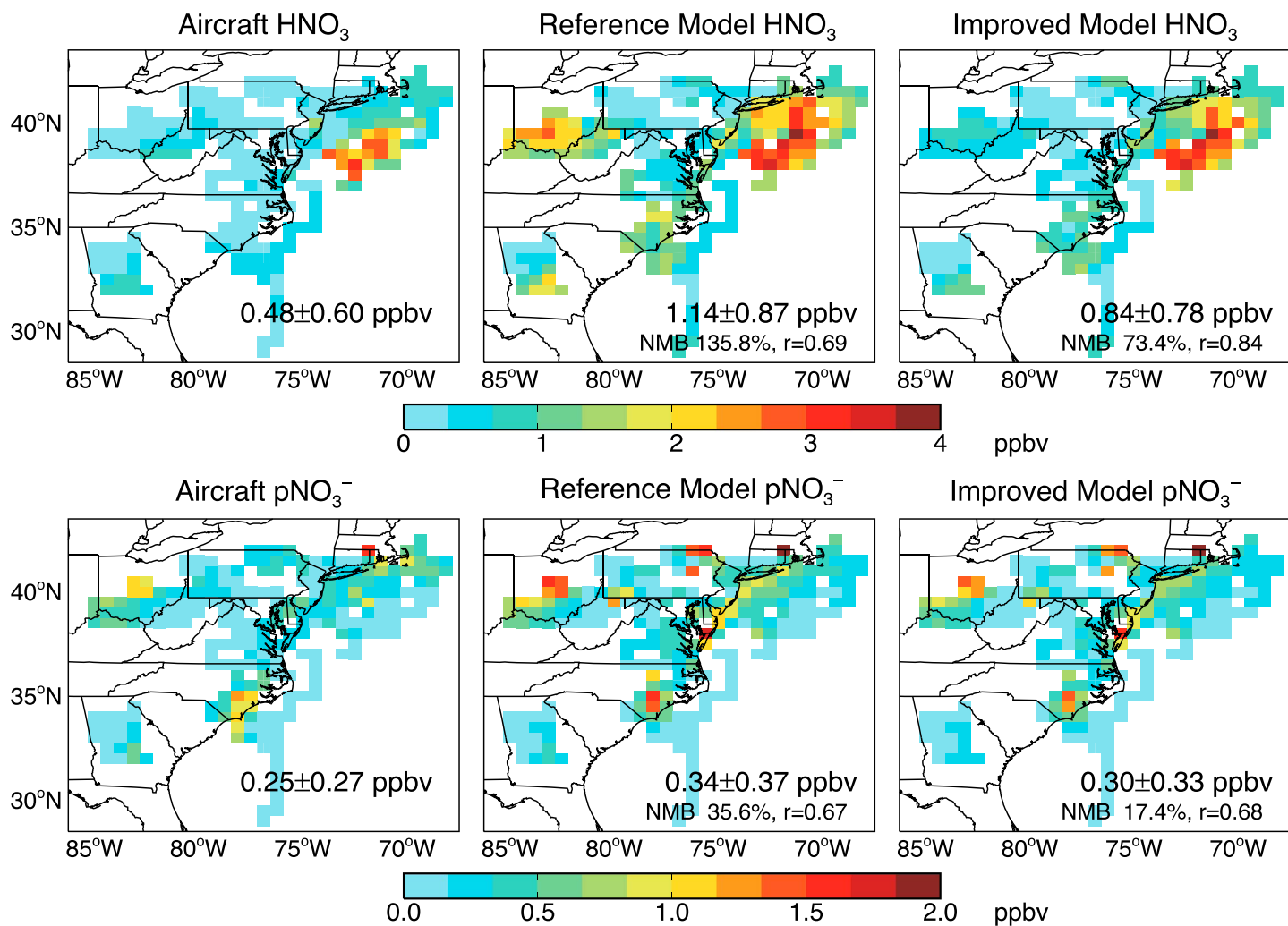
Figure 8. Spatial distribution of HNO$_3$ (top row) and pNO$_3^-$ (bottom row) observed during the WINTER campaign and simulated with GEOS-Chem for altitudes within 1 km of the ground. The observations are averaged over the model grid, and the model is sampled at the time and location of the aircraft. The mean and standard deviations of the concentrations are shown in the insert. NMB = normalized mean bias.

higher, which could potentially reflect a strong seasonal or temperature dependence in the mobile CO/NO$_x$ emission ratio (Salmon et al., 2018).

4.3. Reduction in the HNO$_3$ and pNO$_3^-$ Bias in GEOS-Chem

Previous studies using the GEOS-Chem model have reported a large positive bias in reproducing ground-based observations of pNO$_3^-$ and HNO$_3$ concentrations as well as nitrate wet deposition fluxes over the Eastern United States during winter (Heald et al., 2012; Walker et al., 2012; Zhang et al., 2012), with biases of 50–200%. Implementation of our updated ɣ(N$_2$O$_5$) and v_d (HNO$_3$) leads to lower HNO$_3$ production and increased dry deposition loss, which together result in a significant improvement of the representation of ground-based winter observations of HNO$_3$ and pNO$_3^-$ (Figure 7). Our results are also sensitive to the assumed NH$_3$ emissions from livestock, which we have lowered by a factor of 2 due to the cold temperatures (section 3.2), resulting in lower pNO$_3^-$. The reference GEOS-Chem simulation overestimates CASTNET observations of HNO$_3$ by nearly a factor of 3 (NMB = 168%) for 1 February 1 to 15 March 2015, predicting large HNO$_3$ concentrations (>3 µg/m^3) over the Ohio River Valley and the DC-NYC megalopolis that are not seen by observations (Figures 7a and 7c). The Reference simulation also overestimates surface observations of pNO$_3^-$ from CASTNET, IMPROVE, and CSN for the same period (NMB = 64%, Figures 7d and 7f). In the
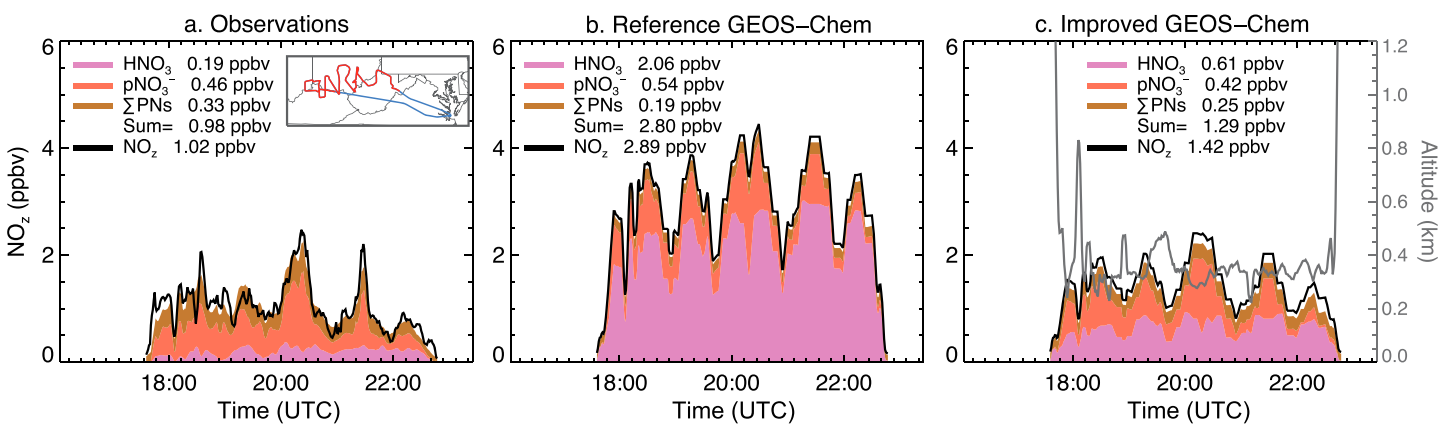
Figure 9. Observed and modeled partitioning of NO_z (=^TNO_y-NO_x) during daytime flight RF02 on 6 February 2015. Time series of HNO_3, pNO_3^-, ΣPNs, and NO_z are shown for (a) observations, (b) the Reference simulation, and (c) the Improved simulation. For each panel the sum of HNO_3, pNO_3^-, ΣPNs is also indicated. The insert in the left panel shows the flight path, with the part highlighted in red corresponding to the time series shown. The altitude of the C-130 is shown with the gray line in panel (c).
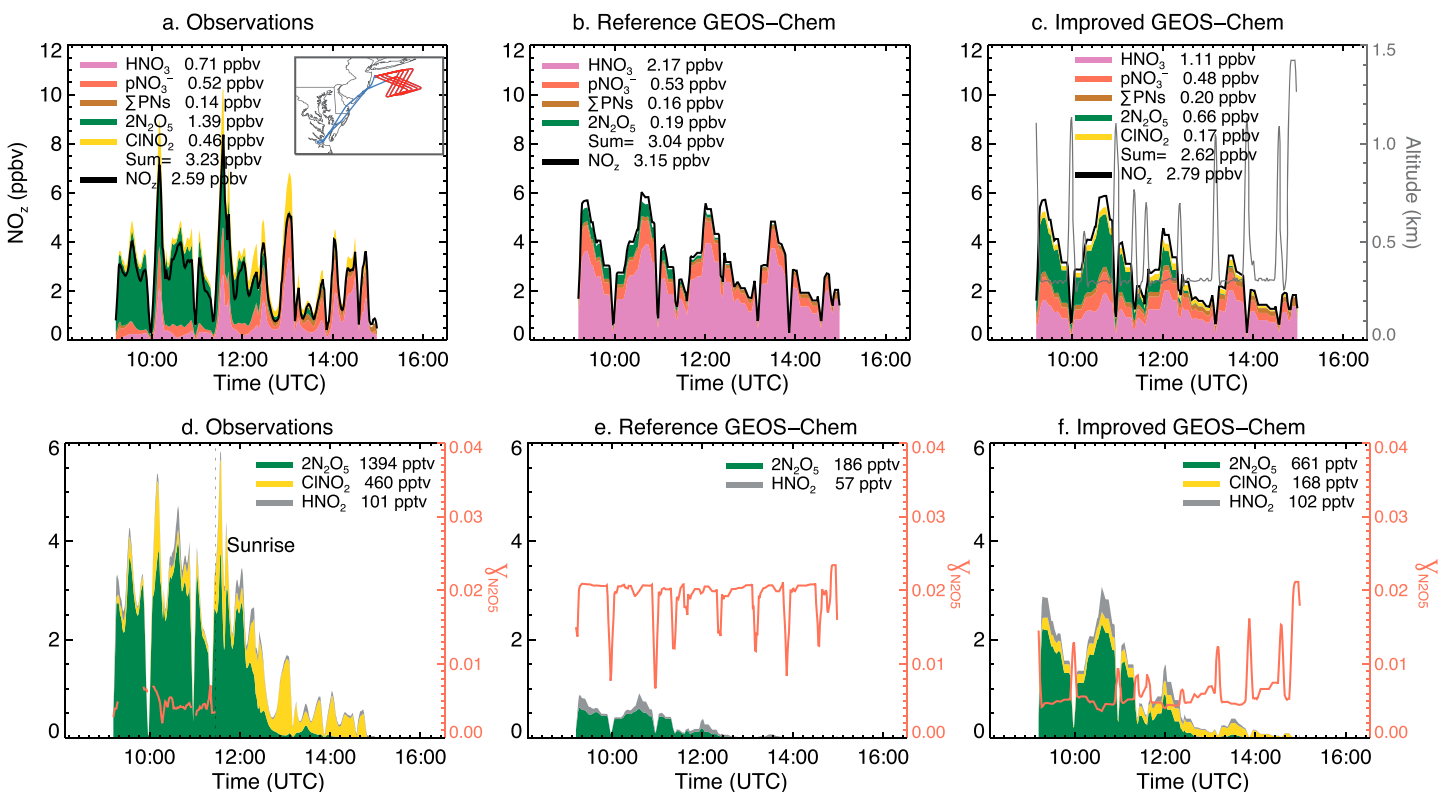

Figure 10. Observed and modeled partitioning of NO_z (=^TNO_y-NO_x) during sunrise flight RF08 on 1 March 2015 (flight track shown in panel a, with time series corresponding to the red part of the track). Time series of HNO_3, pNO_3^-, ΣPNs, $2N_2O_5$, and $ClNO_2$ and NO_z for (a) observations, (b) the Reference simulation, and (c) the Improved simulation. For each panel the sum of individual NO_z species (sum = HNO_3 + pNO_3^- + ΣPNs + $2N_2O_5$ + $ClNO_2$ + HONO) is also indicated. (d–f). Same as (a–c) but for $2N_2O_5$, $ClNO_2$, and HONO. The reactive uptake coefficient for N_2O_5 (γ_{N2O5}) is shown in orange (right axis). The values of γ_{N2O5} in panel (d) are from the box modeling analysis of McDuffie et al. (2018) constrained by WINTER observations, while panels (e) and (f) correspond to the Reference and Improved GEOS-Chem simulations. The altitude of the C-130 is shown with the gray line in panel (c).
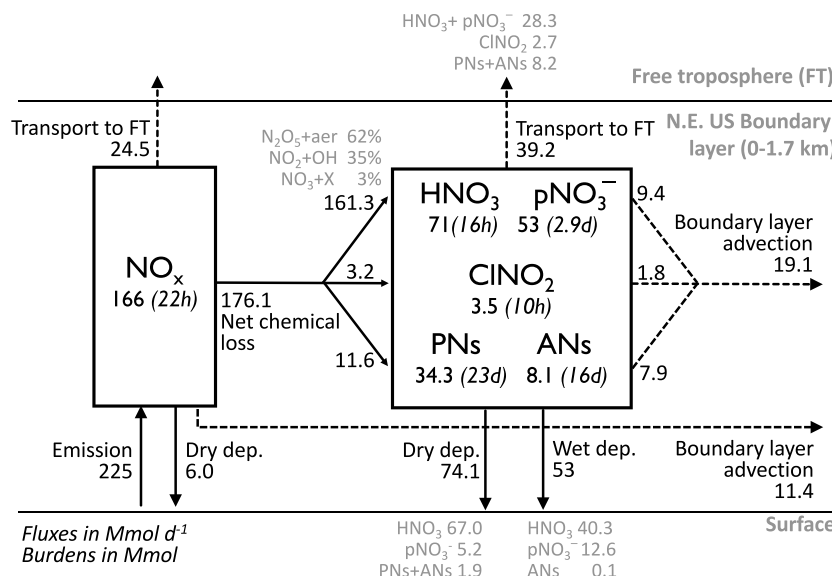
Figure 11. NO_x budget for the NE US boundary layer (defined as 35–45°N, 88.75–65°E, 0–1.7 km) simulated by the Improved GEOS-Chem model during 1 February to 15 March 2015. For each species, we indicate its inventory (in megamoles, Mmol; with 1 Mmol $= 10^6$ moles) and lifetime in parenthesis (in hours or days). In this figure, NO_x is defined as $NO_x = NO + NO_2 + NO_3 + 2N_2O_5 + HONO + HNO_4$. Fluxes are given in megamoles per day. The lifetime of NO_x is defined with respect to chemical loss and deposition, the lifetime of $ClNO_2$ with respect to photolysis, and the lifetime of the other species with respect to deposition. For $HNO_3 + pNO_3^- + ClNO_2 + PNs + ANs$, we give the overall fluxes due to dry deposition, wet deposition, and transport to the free troposphere as well as the individual fluxes (in gray).

Improved simulation, these biases are greatly reduced for surface HNO_3 (NMB = 20%, Figures 7b and 7c) and pNO_3^- (NMB = 35%, Figures 7e and 7f).

Improvements are also seen in the comparison to WINTER aircraft observations of HNO_3 and pNO_3^- (Figures 4 and 8), where the biases below 1 km altitude are reduced by a factor of 2 (NMB decreasing from 136% to 73% for HNO_3 and from 36% to 17% for pNO_3^-). The Improved simulation predicts that the highest HNO_3 concentrations occur over the North Atlantic downwind of the DC-NYC corridor, in agreement with aircraft observations. In contrast, the Reference simulation shows elevated concentrations over the Ohio River Valley, which are not seen in the observations.

Figure 9 displays observations of NO_z ($^T NO_y$-NO_x), as well as individual observations of HNO_3, pNO_3^-, and ΣPNs for RF02, a late afternoon flight taking place on 6 February 2015 during which the C-130 aircraft sampled the region extending over Indiana, Ohio, Kentucky, and West Virginia. We only show the observed time series when the aircraft was below 1 km altitude (highlighted in red on the insert of Figure 9a). Over this source region, observed NO_x accounts for 80–90% of $^T NO_y$. On average, 0.19 ppbv HNO_3, 0.46 ppbv pNO_3^-, and 0.33 ppbv ΣPNs were observed. The Reference simulation displays a +300% bias in $HNO_3 + pNO_3^-$ for this flight, while the bias is reduced to +60% in the Improved simulation (Figure 9c).

An example of the impact of the new $\chi(N_2O_5)$ on nighttime chemistry is illustrated in Figure 10, which shows observations of NO_z during RF08 on 1 March 2015, a night-into-day flight in an hour-glass pattern downwind of the DC-NYC region. Sunrise took place at 12 UTC (7 a.m. local time). Observed nighttime NO_z is dominated by N_2O_5, with little contributions from $HNO_3 + pNO_3^-$ (<1 ppbv). The Reference simulation predicts rapid heterogeneous conversion of N_2O_5 to HNO_3 ($\chi(N_2O_5) \sim 0.02$) resulting in a factor of 3 overestimate in $HNO_3 + pNO_3^-$ (Figure 10b). In the Improved simulation, $\chi(N_2O_5)$ decreases to 0.005 as a result of the pNO_3^- inhibition on SNA and the low $\chi(N_2O_5)$ assumed for OA. This leads to a factor of 2.5 decrease in HNO_3, a factor of 3 increase in N_2O_5, and better agreement with the observed partitioning (Figures 10c and 10f). Figure 10d shows the $\chi(N_2O_5)$ calculated by the iterative box modeling analysis of McDuffie et al. (2018), who found $\chi(N_2O_5) = 0.0046 \pm 0.0013$ (flight average ± standard deviation, 60-s average data) for this flight, consistent with our parameterization in the Improved simulation: $\chi(N_2O_5) = 0.0049 \pm 0.0006$. The

Table 2

NO_x Budget Over the Northeast United States[a] for 1 February to 15 March 2015 in the Improved GEOS-Chem Simulation

Budget term	Northeast United States
Surface NO_x emissions[b], Mmol/day	225.0
NO_x chemical loss, Mmol/day	176.1
N_2O_5 + aerosols	103.7 (58%)
NO_2 + OH	56.9 (33%)
NO_2 + aerosols/NO_3 + VOCs	3.9 (2%)
PNs production	9.6 (6%)
ANs production	2.0 (1%)
Dry deposition, Mmol/day	80.1
NO_x	6.0
HNO_3	67.0
pNO_3^-	5.2
PNs	1.5
ANs	0.4
Wet deposition, Mmol/day	53.0
HNO_3	40.3
pNO_3^-	12.6
ANs	0.1
Net export[c], Mmol/day	94.2
NO_x	35.9
HNO_3 + pNO_3^-	37.7
PNs	13.8
ANs	2.3
$ClNO_2$	4.5
Lifetimes[d], days	2.53
NO_x	0.91
HNO_3 + pNO_3^-	0.95
PNs	22.9
ANs	16.2
$ClNO_2$	0.43
Burden, Mmol	337.0
NO_x	166.5
HNO_3	71.2
pNO_3^-	53.2
PNs	34.4
ANs	8.2
$ClNO_2$	3.5

Note. In this table, NO_x is defined as NO_x = NO +NO_2 + NO_3 + $2N_2O_5$ + HONO + HNO_4. PN = peroxy acyl nitrate; AN = alkyl nitrate; Mmol = Megamole, with 1 Mmol = 10^6 moles.
[a]The Northeast United States is defined as 35–45°N; 88.75–65°W; 0–1.7 km, including both land and water.   [b]NO_x emissions include shipping emissions in coastal waters.   [c]Net export refers to net transport out of the domain (including horizontal and vertical transport). It is defined as positive for a net flux out.   [d]The NO_x lifetime is defined against chemical loss and deposition, the lifetime of $ClNO_2$ is defined against photolysis, while the lifetime for other species is defined with respect to deposition.

campaign wide comparison of $\gamma(N_2O_5)$ between the box model and Improved GEOS-Chem simulation is shown in Figure S24 of the supporting information in McDuffie et al. (2018).

The Improved simulation predicts ~100 to 300 pptv $ClNO_2$, significantly lower than observed values of $ClNO_2$, which varied between 200 and >1,000 pptv for this flight (Figure 10d). More generally, we find that GEOS-Chem underestimates $ClNO_2$ by a factor of 2 during the WINTER campaign (Figure 4). This suggests that the GEOS-Chem $\phi(ClNO_2)$ values are too low, likely related to an underestimate in pCl^- concentrations as we neglect anthropogenic sources of chlorine in this simulation (section 3.3.3) and potential repartitioning of coarse mode sea salt chloride to the fine mode population. Indeed, our assumption that 10% of pCl^- from submicron sea salt is displaced onto SNA aerosol results in median PM_1 pCl^- mixing ratios of 5 pptv (<1 km) in GEOS-Chem, which is a factor of 2 lower than the median nonrefractory PM_1 pCl^- observed by the HR-ToF-AMS during WINTER. This underestimate in $\phi(ClNO_2)$ means that we underestimate NO_x recycling via $ClNO_2$ thus producing too much HNO_3 and could potentially explain some of the remaining model overestimate of HNO_3 and underestimate in NO_x.

The remaining model overestimate of HNO_3/NO_x could also be the result of an overestimate in $\gamma(N_2O_5)$ in GEOS-Chem, as we treat aerosols as liquid and externally mixed. At low RH, solid NH_4HSO_4, or $(NH_4)_2SO_4$ particles can be present, and organic aerosol can transition to solid or semisolid state (Seinfeld & Pandis, 2006; Shiraiwa et al., 2017; Song et al., 2016). Solid or semisolid particles at low RH (<30–50%) tend to have much lower $\gamma(N_2O_5)$, typically less than 0.001 (e.g., Abbatt et al., 2012; Davis et al., 2008, and references therein). During nighttime WINTER flights below 1 km altitude, mean observed RH was 48%, with 28% of observations displaying RH values below 30%. In our $\gamma(N_2O_5)$ parameterization and aerosol surface area calculation, we assume that aerosols remain liquid and do not account for the occurrence of solid or semisolid particles. In addition, laboratory measurements have shown that organic coatings on inorganic aerosol can lower $\gamma(N_2O_5)$ (e.g., Anttila et al., 2006; Gaston et al., 2014). As we treat aerosol as externally mixed, we do not take this effect into account.

Another possibility is an overly fast daytime production of HNO_3 related either to a model overestimate in OH concentrations or in the OH + NO_2 kinetic rate constant. GEOS-Chem uses the rate constant recommended by the NASA Jet Propulsion Laboratory panel evaluation (Sander et al., 2011). Several studies have suggested that this rate constant might be 15–20% lower than the value recommended by Jet Propulsion Laboratory (Henderson et al., 2012; Mollner et al., 2010). As no measurements of OH, HO_2, or H_2O_2 were made as part of WINTER, we cannot directly evaluate our modeled OH concentrationss. However, our simulation does reproduce WINTER observations of HO_x precursors (H_2O, O_3, HCHO, and HONO) and controlling species (NO_x, CO) relatively well, providing indirect evidence that our modeled HO_x concentrations are likely reasonable. Furthermore, Schroder et al. (2018) estimated OH concentrations from the relative decay of pairs of hydrocarbons during WINTER, also finding levels consistent with those in GEOS-Chem.

4.4. ^TNO_y Budget Over the NE US During Winter

Figure 11 and Table 2 present the budget of ^TNO_y in the Improved GEOS-Chem simulation for the NE US (35–45°N, 88.75–65°W, and 0–1.7 km). Half of the ^TNO_y burden is in the form of NO_x (defined in this

Table 3
Nitrogen Deposition (Mg N/Month) Over Land Over the Northeast United State for 1 February to 15 March 2015 in the Improved GEOS-Chem Simulation

Deposition process	Northeast United States[a]
Wet HNO_3	23.3
Dry HNO_3	18.6
Wet pNO_3^-	5.3
Dry NO_2	2.0
Dry pNO_3^-	1.6
Dry PNs	0.48
Dry N_2O_5	0.30
Dry ANs	0.12
Wet ANs	0.04
Total NO_y wet deposition	28.6
Total NO_y dry deposition	23.1
Total NO_y deposition	51.7
Wet NH_4^+	13.0
Dry NH_3	2.8
Dry NH_4^+	2.8
Wet NH_3	0.9
Total NH_x wet deposition	13.9
Total NH_x dry deposition	5.6
Total NH_x deposition	19.5

Note. PN = peroxy acyl nitrate; AN = alkyl nitrate.
[a]The Northeast United States is defined as the land area bounded by 35–45°N; 88.75–65°W.

section as $NO_x = NO+NO_2 + NO_3 + 2N_2O_5 + HONO + HNO_4$), with 37% being present as $HNO_3 + pNO_3^-$, 12% as organic nitrates, and 1% as $ClNO_2$. GEOS-Chem predicts that 43% of $HNO_3 + pNO_3^-$ is in the form of pNO_3^-, similar to the observed value of 48% (Guo et al., 2016). This indicates that the pH of aerosol is simulated reasonably well in GEOS-Chem (as noted in section 4.1), since partitioning of nitrate between the gas and particle phases is highly sensitive to pH when nearly equal concentrations are found in the two phases (Guo et al., 2016; Shah et al., 2018).

We can contrast this ^TNO_y partitioning to summertime aircraft observations and model simulations reported by Hudman et al. (2007) for the 2004 ICARTT campaign over the NE US. They find that below 2 km altitude, NO_x, HNO_3, and PAN accounted for 18%, 62%, and 20% of NO_y, respectively. The slow photochemistry during winter thus shifts the partitioning strongly in favor of NO_x, reducing the relative importance of HNO_3 and PAN. Our partitioning for WINTER is generally similar to the seasonal modeling study of Liang et al. (1998) for winter (December, January, February)-spring (March, April, May) over the continental United States, which calculated 61–40% NO_x, 27–32% as $HNO_3 + pNO_3^-$, and 12–28% as PAN.

In the GEOS-Chem simulation, the lifetime of NO_x against oxidation and deposition is 22 hr. We find that 91% of NO_x is oxidized to produce HNO_3, with 7% producing organic nitrates, and 2% $ClNO_2$ (Table 2 and Figure 11). While organic nitrates have the longest lifetimes of all NO_y species (23 days for PNs and 16 days for ANs), their production is very slow because of low biogenic VOC emissions. We find that nighttime N_2O_5 heterogeneous chemistry accounts for 62% of HNO_3 production, with 35% due to daytime oxidation by reaction of NO_2 with OH and 3% from reactions of NO_3 with VOCs.

Based on WINTER observations of the evolution of NO_x concentrations in the U.S. East Coast boundary layer outflow, Kenagy et al. (2018) calculate an *e*-folding NO_x lifetime of 29 hr for daytime and 6.3 hr for nighttime. This corresponds to a daily mean lifetime of 10 hr (taking into account the 10h45min length of day) and includes NO_x loss due to chemistry, deposition, and transport to the free troposphere. Taking these three processes into account, we calculate a NO_x lifetime of 19 hr based on Table 2 and Figure 11. If we further examine the NO_x budget in GEOS-Chem restricted to 0–800 m in the oceanic outflow, similar to the domain used by Kenagy et al. (2018), the NO_x lifetime decreases to 11 hr due to enhanced turbulent mixing between 0 and 800 m and the overlaying atmosphere. Kenagy et al. (2018) infer a dry deposition lifetime of HNO_3 of 23 hr over the ocean (29 hr during the day and 20 hr at night), similar to the HNO_3 dry deposition lifetime calculated in GEOS-Chem (25 hr, Table 2).

With the GEOS-Chem simulation, we find that 42% of the NO_x emitted in the NE US is exported out of the domain (Table 2). Figure 11 shows that export by transport to the free troposphere (63.7 Mmol/day, with 1 Mmol = 10^6 moles) is twice as large as export via boundary layer advection (30.6 Mmol/day). Export of ^TNO_y during WINTER is composed of 38% NO_x, 40% $HNO_3 + pNO_3^-$, 17% organic nitrates, and 5% $ClNO_2$. We can compare our WINTER NO_x free tropospheric export efficiency of 28% (defined as the ratio of free troposphere NO_y export/NO_x emissions = 63.7 Mmol per day/225 Mmol per day) to values based on analysis of aircraft observations during other seasons. For the July–August ICARTT observations above 2.5 km altitude, Hudman et al. (2007) report an export efficiency of 16% composed of 13% NO_x, 47% HNO_3, and 42% PAN. Based on aircraft observations obtained during the NARE campaign in September 1997 downwind of the NE US, Li et al. (2004) and Parrish et al. (2004) find an export efficiency of 15–20%, with 6–8% as NO_x, 52–57% as HNO_3, and 34–36% as PAN. Thus, as expected from a longer NO_x lifetime, the NO_y export efficiency during WINTER is significantly larger than in other seasons. Furthermore, while PAN plays a significant role in NO_y export during summer and fall, it is of minor importance during winter and is replaced by a larger role for direct NO_x export from the boundary layer. The 3-D modeling study of Liang et al. (1998) reports a 34–26%
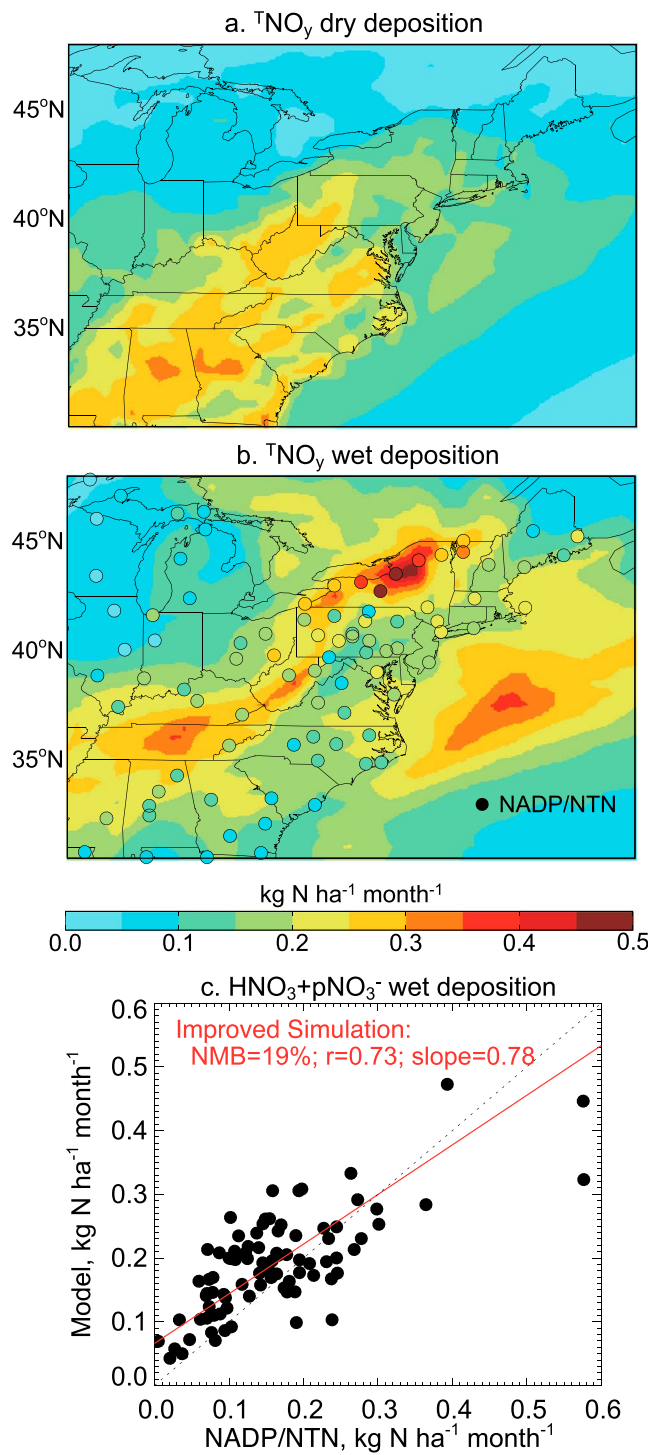
a. ^TNO_y dry deposition

b. ^TNO_y wet deposition

● NADP/NTN

kg N ha^{-1} month^{-1}

0.0   0.1   0.2   0.3   0.4   0.5

c. HNO_3+pNO_3^- wet deposition

Improved Simulation:
NMB=19%; r=0.73; slope=0.78

Model, kg N ha^{-1} month^{-1}

NADP/NTN, kg N ha^{-1} month^{-1}

Figure 12. GEOS-Chem mean monthly ^TNO_y (a) dry deposition and (b) wet deposition fluxes in the Improved Simulation for the period of the WINTER experiment (1 February to 15 March, 2015) in units of kilogram nitrogen per hectare per month. Also shown on panel (b) are the weekly NADP/NTN HNO_3 + pNO_3^- wet deposition flux observations for that period. (c) Scatter plot of modeled and observed HNO_3 + pNO_3^- wet deposition. NADP/NTN = National Atmospheric Deposition Program/National Trends Network.

NO_y export efficiency for winter-spring, lower than our 42%. We attribute this difference to the higher $ɣ(N_2O_5) = 0.1$ used in Liang et al. (1998) and thus faster HNO_3 production and scavenging prior to export.

4.5. Nitrogen Deposition

Table 3 summarizes the main forms of ^TNO_y deposition over land for the NE US during the 1 February to 15 March 2015 period. The wet deposition values in Table 3 are only over land and include scavenging from the entire troposphere, while values in Table 2 are for both land and ocean but only include scavenging below 1.7 km. Over the NE US in the Improved simulation, we find that ^TNO_y deposition is dominated by wet deposition of HNO_3 and dry deposition of HNO_3, which account for 45% and 36% of the ^TNO_y deposition flux (51.7 Mg N/month, with 1 Mg = 10^6 g). Other contributions are from wet deposition of pNO_3^- (10%), dry deposition of NO_2 (3.9%), and dry deposition of pNO_3^- (3.1%; Table 3). Wet and dry deposition accounts for 55% and 45% of the ^TNO_y deposition flux, respectively. ^TNO_y deposition over the NE US is responsible for a third of the deposition over the contiguous US, following the distribution of NO_x emissions.

Compared to the Reference simulation (Table S2), the Improved simulation leads to a 15% decrease in the ^TNO_y wet deposition flux and a 48% increase in the dry deposition flux, thus shifting deposition from wet to dry such that they both contribute to similar amounts of deposition with little change to the total deposition flux (Reference: 49.1 Mg N/month; Improved: 51.7 Mg N/month; Tables 3 and S3).

Figure 12 shows the spatial distribution of ^TNO_y dry and wet deposition for 1 February to 15 March 2015 as calculated in the Improved GEOS-Chem simulation. Dry deposition of ^TNO_y is dominated by HNO_3 (Table 3 and Figure 12a) and follows the spatial distribution of surface HNO_3, which displays relatively uniform concentrations (Figure 7b) and hence uniform dry deposition fluxes throughout the Eastern United States. Wet deposition of ^TNO_y follows the distribution of precipitation, which is enhanced along the Appalachian Mountains (Figure 12b). Figure 12c compares the observed HNO_3 + pNO_3^- wet deposition flux at NADP/NTN sites to the Improved simulation, showing that on average the GEOS-Chem model overestimate deposition by 19%, in line with our findings of a 20–30% overestimate in HNO_3 concentrations both based on ground-based observations and aircraft observations. The Reference simulation displays a larger positive bias of 37% for wet deposition (not shown). The Improved simulation reproduces the maximum in wet deposition observed over upstate New York. Table 3 also lists the ammonia (NH_3) and ammonium aerosol (NH_4^+) deposition fluxes, which contribute to 27% of the total nitrogen deposition fluxes. The spatial distribution of the total nitrogen deposition flux shows nearly equal contributions of wet and dry deposition fluxes over land but a dominant role for wet deposition over the ocean (Figure S2).

5. Conclusions

In this work, we have presented a detailed analysis of the chemistry and budget of reactive nitrogen species in the lower troposphere over the NE US, using observations from the WINTER aircraft campaign, concurrent surface observations, and the GEOS-Chem chemical transport model. We found a factor of 2 underestimate of aircraft and ground-based

observations of HCHO, which can be eliminated with a fivefold increase in primary emissions of HCHO in the NEI emission inventory, potentially associated with an underestimate in primary HCHO from cold start mobile emissions and RWC. Past studies conducted during summer or warm U.S. regions have reported very large overestimates of NO_x emissions in the NEI inventory. Unlike these studies, we found that the NEI NO_x emission inventory is consistent with WINTER ^TNO_y to within better than 10%. This suggests potential issues with the NEI seasonal dependence of anthropogenic NO_x emissions or a bias in the models' representations of summertime PBL mixing and/or chemistry. Furthermore, based on observed CO/NO_x enhancement ratios, we found that the NEI inventory overestimates CO emissions by 60–90% over the NE US.

Updates to the dry deposition velocity, to $\chi(N_2O_5)$, including its dependence on nitrate and organic aerosol, and a good representation of PM_1 pH result in a significant reduction of the long-standing HNO_3 and pNO_3^- overestimate in GEOS-Chem. For ground-based observations, the model HNO_3 bias is reduced from +168% to +20%, while the pNO_3^- bias is reduced from +64% to +30%. For aircraft observations, the HNO_3 and pNO_3^- bias is reduced by a factor of 2 (down to 73% and 17%, respectively). The remaining overestimate HNO_3 and pNO_3^-, combined with a 25–50% underestimate in NO_x, N_2O_5, and $ClNO_2$, could be due to a combination of the following three potential factors: (i) too low values for $\phi(ClNO_2)$, (ii) a suppression of $\chi(N_2O_5)$ on solid or semisolid aerosol particles or on internally mixed inorganic and organic particles, and (iii) an overestimate of the daytime production of HNO_3 via OH + NO_2. In order to resolve these remaining issues, wintertime measurements of HO_x and H_2O_2 as well as particle hygroscopicity or morphology would be necessary in addition to the suite of detailed NO_y and aerosol speciation measurements obtained during WINTER.

The slow rate of NO_x oxidation chemistry during winter results in a 22 hr lifetime over the NE US, and half of ^TNO_y present as NO_x below 1 km altitude over the NE US with the remaining 37% as $HNO_3 + pNO_3^-$ and 13% mostly as PAN. Nighttime heterogeneous uptake of N_2O_5 accounts for 58% of NO_x chemical loss, while daytime reaction of NO_2 with OH leads to 33% of the loss. We find a 42% export efficiency of NO_x emissions from the NE US, mostly in the form of NO_x and $HNO_3 + pNO_3^-$. Over land in the NE US, wet and dry deposition accounts for 55% and 45% of the NO_y deposition flux, respectively, with 94% of ^TNO_y deposition associated with HNO_3 and pNO_3^-.

The extensive WINTER airborne observations targeted emissions and their chemical transformation within the boundary layer, in a specific region and season, with flights encompassing both daytime and nighttime. This provides a model for future aircraft campaigns aimed at different seasons and regions. The chemical and dynamical processes taking place in the boundary layer remain missing links in our understanding of the fate of pollutants within the first few hour-days after they are being emitted.

References

Abbatt, J. P. D., Lee, A. K. Y., & Thornton, J. A. (2012). Quantifying trace gas uptake to tropospheric aerosol: Recent advances and remaining challenges. *Chemical Society Reviews*, *41*(19), 6555–6581. https://doi.org/10.1039/C2CS35052A

Alexander, B., Hastings, M. G., Allman, D. J., Dachs, J., Thornton, J. A., & Kunasek, S. A. (2009). Quantifying atmospheric nitrate formation pathways based on a global model of the oxygen isotopic composition (Δ^{17}O) of atmospheric nitrate. *Atmospheric Chemistry and Physics*, *9*(14), 5043–5056. https://doi.org/10.5194/acp-9-5043-2009

Amos, H. M., Jacob, D. J., Holmes, C. D., Fisher, J. A., Wang, Q., Yantosca, R. M., et al. (2012). Gas-particle partitioning of atmospheric Hg (II) and its effect on global mercury deposition. *Atmospheric Chemistry and Physics*, *12*(1), 591–603. https://doi.org/10.5194/acp-12-591-2012

Aneja, V. P., Chauhan, J. P., & Walker, J. T. (2000). Characterization of atmospheric ammonia emissions from swine waste storage and treatment lagoons. *Journal of Geophysical Research*, *105*(D9), 11,535–11,545. https://doi.org/10.1029/2000JD900066

Anderson, D. C., Loughner, C. P., Diskin, G., Weinheimer, A., Canty, T. P., Salawitch, R. J., et al. (2014). Measured and modeled CO and NO_y in DISCOVER-AQ: An evaluation of emissions and chemistry over the eastern US. *Atmospheric Environment*, *96*, 78–87. https://doi.org/10.1016/j.atmosenv.2014.07.004

Anttila, T., Kiendler-Scharr, A., Tillmann, R., & Mentel, T. F. (2006). On the reactive uptake of gaseous compounds by organic-coated aqueous aerosols: Theoretical analysis and application to the heterogeneous hydrolysis of N_2O_5. *The Journal of Physical Chemistry A*, *110*(35), 10,435–10,443. https://doi.org/10.1021/jp062403c

Appel, K. W., Napelenok, S. L., Foley, K. M., Pye, H. O. T., Hogrefe, C., Luecken, D. J., et al. (2017). Description and evaluation of the Community Multiscale Air Quality (CMAQ) modeling system version 5.1. *Geoscientific Model Development*, *10*(4), 1703–1732. https://doi.org/10.5194/gmd-10-1703-2017

Badger, C. L., Griffiths, P. T., George, I., Abbatt, J. P. D., & Cox, R. A. (2006). Reactive uptake of N_2O_5 by aerosol particles containing mixtures of humic acid and ammonium sulfate. *Journal of Physical Chemistry A*, *110*(21), 6986–6994. https://doi.org/10.1021/jp0562678

Behnke, W., George, C., Scheer, V., & Zetzsch, C. (1997). Production and decay of $ClNO_2$ from the reaction of gaseous N_2O_5 with NaCl solution: Bulk and aerosol experiments. *Journal of Geophysical Research*, *102*(D3), 3795–3804. https://doi.org/10.1029/96JD03057

Bertram, T. H., & Thornton, J. A. (2009). Toward a general parameterization of N_2O_5 reactivity on aqueous particles: The competing effects of particle liquid water, nitrate and chloride. *Atmospheric Chemistry and Physics*, *9*(21), 8351–8363. https://doi.org/10.5194/acp-9-8351-2009

Bertram, T. H., Thornton, J. A., Riedel, T. P., Middlebrook, A. M., Bahreini, R., Bates, T. S., et al. (2009). Direct observations of N_2O_5 reactivity on ambient aerosol particles. *Geophysical Research Letters*, *36*, L19803. https://doi.org/10.1029/2009GL040248

Bey, I., Jacob, D. J., Yantosca, R. M., Logan, J. A., Field, B. D., Fiore, A. M., et al. (2001). Global modeling of tropospheric chemistry with assimilated meteorology: Model description and evaluation. *Journal of Geophysical Research*, *106*(D19), 23,073–23,095. https://doi.org/10.1029/2001JD000807

Brioude, J., Angevine, W. M., Ahmadov, R., Kim, S.-W., Evan, S., McKeen, S. A., et al. (2013). Top-down estimate of surface flux in the Los Angeles Basin using a mesoscale inverse modeling technique: assessing anthropogenic emissions of CO, NO_x and CO_2 and their impacts. *Atmospheric Chemistry and Physics*, *13*(7), 3661–3677. https://doi.org/10.5194/acp-13-3661-2013

Brown, S. S., Dubé, W. P., Fuchs, H., Ryerson, T. B., Wollny, A. G., Brock, C. A., et al. (2009). Reactive uptake coefficients for N_2O_5 determined from aircraft measurements during the Second Texas Air Quality Study: Comparison to current model parameterizations. *Journal of Geophysical Research*, *114*, D00F10. https://doi.org/10.1029/2008JD011679

Brown, S. S., & Stutz, J. (2012). Nighttime radical observations and chemistry. *Chemical Society Reviews*, *41*(19), 6405–6447. https://doi.org/10.1039/C2CS35181A.

Canty, T. P., Hembeck, L., Vinciguerra, T. P., Anderson, D. C., Goldberg, D. L., Carpenter, S. F., et al. (2015). Ozone and NO_x chemistry in the eastern US: Evaluation of CMAQ/CB05 with satellite (OMI) data. *Atmospheric Chemistry and Physics*, *15*(19), 10,965–10,982. https://doi.org/10.5194/acp-15-10965-2015

Cazorla, M., Wolfe, G. M., Bailey, S. A., Swanson, A. K., Arkinson, H. L., & Hanisco, T. F. (2015). A new airborne laser-induced fluorescence instrument for in situ detection of formaldehyde throughout the troposphere and lower stratosphere. *Atmospheric Measurement Techniques*, *8*(2), 541–552. https://doi.org/10.5194/amt-8-541-2015

Colette, A., Granier, C., Hodnebrog, Ø., Jakobs, H., Maurizi, A., Nyiri, A., et al. (2011). Air quality trends in Europe over the past decade: A first multi-model assessment. *Atmospheric Chemistry and Physics*, *11*(22), 11,657–11,678. https://doi.org/10.5194/acp-11-11657-2011

Croft, B., Martin, R. V., Leaitch, W. R., Tunved, P., Breider, T. J., D'Andrea, S. D., & et al. (2016). Processes controlling the annual cycle of Arctic aerosol number and size distributions. *Atmospheric Chemistry and Physics*, *16*(6), 3665–3682. https://doi.org/10.5194/acp-16-3665-2016

Davis, J. M., Bhave, P. V., & Foley, K. M. (2008). Parameterization of N_2O_5 reaction probabilities on the surface of particles containing ammonium, sulfate, and nitrate. *Atmospheric Chemistry and Physics*, *8*(17), 5295–5311. https://doi.org/10.5194/acp-8-5295-2008

DeCarlo, P. F., Kimmel, J. R., Trimborn, A., Northway, M. J., Jayne, J. T., Aiken, A. C., et al. (2006). Field-deployable, high-resolution, time-of-flight aerosol mass spectrometer. *Analytical Chemistry*, *78*(24), 8281–8289. https://doi.org/10.1021/ac061249n

Demerjian, K. L. (2000). A review of national monitoring networks in North America. *Atmospheric Environment*, *34*(12-14), 1861–1884. https://doi.org/10.1016/S1352-2310(99)00452-5

Dentener, F., & Crutzen, P. (1993). Reaction of N_2O_5 on tropospheric aerosols: Impact on the global distributions of NO_x, O_3, and OH. *Journal of Geophysical Research*, *98*(D4), 7149–7163. https://doi.org/10.1029/92jd02979

Dubé, W. P., Brown, S. S., Osthoff, H. D., Nunley, M. R., Ciciora, S. J., Paris, M. W., et al. (2006). Aircraft instrument for simultaneous, in situ measurement of NO_3 and N_2O_5 via pulsed cavity ring-down spectroscopy. *Review of Scientific Instruments*, *77*(3), 034101. https://doi.org/10.1063/1.2176058

Duncan, B. N., Lamsal, L. N., Thompson, A. M., Yoshida, Y., Lu, Z., Streets, D. G., et al. (2016). A space-based, high-resolution view of notable changes in urban NO_x pollution around the world (2005–2014). *Journal of Geophysical Research: Atmospheres*, *121*, 976–996. https://doi.org/10.1002/2015JD024121

Dunlea, E. J., Herndon, S. C., Nelson, D. D., Volkamer, R. M., San Martini, F., Sheehy, P. M., et al. (2007). Evaluation of nitrogen dioxide chemiluminescence monitors in a polluted urban environment. *Atmospheric Chemistry and Physics*, *7*(10), 2691–2704. https://doi.org/10.5194/acp-7-2691-2007

Ellis, R. A., Jacob, D. J., Sulprizio, M. P., Zhang, L., Holmes, C. D., Schichtel, B. A., et al. (2013). Present and future nitrogen deposition to national parks in the United States: Critical load exceedances. *Atmospheric Chemistry and Physics*, *13*(17), 9083–9095. https://doi.org/10.5194/acp-13-9083-2013

Environmental Protection Agency (2017). Air pollutant emissions trends data. Available at: https://www.epa.gov/air-emissions-inventories/air-pollutant-emissions-trends-data [Accessed June 1, 2017].

Erisman, J. W., van Pul, A., & Wyers, P. (1994). Parameterization of dry deposition mechanisms for the quantification of atmospheric input to ecosystems. *Atmospheric Environment*, *28*(16), 2595–2607. https://doi.org/10.1016/1352-2310(94)90433-2

Evans, M. J., & Jacob, D. J. (2005). Impact of new laboratory studies of N_2O_5 hydrolysis on global model budgets of tropospheric nitrogen oxides, ozone, and OH. *Geophysical Research Letters*, *32*, D00F10. https://doi.org/10.1029/2005GL022469

Fibiger, D. L., McDuffie, E. E., Dubé, W. P., Aikin, K. C., Lopez-Hilfiker, F. D., Lee, B. H., et al. (2018). Wintertime overnight NO_x removal in a Southeastern United States coal-fired power plant plume: A model for understanding winter NO_x processing and its implications. *Journal of Geophysical Research: Atmospheres*, *123*, 1412–1425. https://doi.org/10.1002/2017JD027768

Finlayson-Pitts, B. J., Ezell, M. J., & Pitts, J. N. (1989). Formation of chemically active chlorine compounds by reactions of atmospheric NaCl particles with gaseous N_2O_5 and $ClONO_2$. *Nature*, *337*(6204), 241–244. https://doi.org/10.1038/337241a0

Finlayson-Pitts, B. J., Wingen, L. M., Sumner, A. L., Syomin, D., & Ramazan, K. A. (2003). The heterogeneous hydrolysis of NO_2 in laboratory systems and in outdoor and indoor atmospheres: An integrated mechanism. *Physical Chemistry Chemical Physics*, *5*(2), 223–242. https://doi.org/10.1039/b208564j

Fisher, J. A., Jacob, D. J., Travis, K. R., Kim, P. S., Marais, E. A., Chan Miller, C., et al. (2016). Organic nitrate chemistry and its implications for nitrogen budgets in an isoprene- and monoterpene-rich atmosphere: Constraints from aircraft (SEAC4RS) and ground-based (SOAS) observations in the Southeast US. *Atmospheric Chemistry and Physics*, *16*(9), 5969–5991. https://doi.org/10.5194/acp-16-5969-2016

Fountoukis, C., & Nenes, A. (2007). ISORROPIA II: A computationally efficient thermodynamic equilibrium model for K^+–Ca^{2+}–Mg^{2+}–NH_4^+–Na^+–SO_4^{2-}–NO_3^-–Cl^-–H_2O aerosols. *Atmospheric Chemistry and Physics*, *7*, 4639–4659. https://doi.org/10.5194/acp-7-4639-2007

Fuchs, H., Dube, W. P., Lerner, B. M., Wagner, N. L., Williams, E. J., & Brown, S. S. (2009). A sensitive and versatile detector for atmospheric NO_2 and NO_x based on blue diode laser cavity ring-down spectroscopy. *Environmental Science & Technology*, *43*(20), 7831–7836. https://doi.org/10.1021/es902067h

Fujita, E. M., Campbell, D. E., Zielinska, B., Chow, J. C., Lindhjem, C. E., DenBleyker, A., et al. (2012). Comparison of the MOVES2010a, MOBILE6.2, and EMFAC2007 mobile source emission models with on-road traffic tunnel and remote sensing measurements. *Journal of Air Waste Management*, *62*(10), 1134–1149. https://doi.org/10.1080/10962247.2012.699016

Fuzzi, S., Decesari, S., Facchini, M. C., Matta, E., Mircea, M., & Tagliavini, E. (2001). A simplified model of the water soluble organic component of atmospheric aerosols. *Geophysical Research Letters*, *28*, 4079–4082. https://doi.org/10.1029/2001GL013418

Gaston, C. J., Thornton, J. A., & Ng, N. L. (2014). Reactive uptake of N_2O_5 to internally mixed inorganic and organic particles: The role of organic carbon oxidation state and inferred organic phase separations. *Atmospheric Chemistry and Physics*, *14*(11), 5693–5707. https://doi.org/10.5194/acp-14-5693-2014

Gerbig, C., Schmitgen, S., Kley, D., Volz-Thomas, A., Dewey, K., & Haaks, D. (1999). An improved fast-response vacuum-UV resonance fluorescence CO instrument. *Journal of Geophysical Research*, *104*(D1), 1699–1704. https://doi.org/10.1029/1998JD100031

Ghosh, B., Papanastasiou, D. K., Talukdar, R. K., Roberts, J. M., & Burkholder, J. B. (2012). Nitryl chloride (ClNO$_2$): UV/Vis absorption spectrum between 210 and 296 K and O(^{3}P) quantum yield at 193 and 248 nm. *Journal of Physical Chemistry A*, *116*(24), 5796–5805. https://doi.org/10.1021/jp207389y

Gilliland, A. B., Appel, K. W., Pinder, R. W., & Dennis, R. L. (2006). Seasonal NH$_3$ emissions for the continental United States: Inverse model estimation and evaluation. *Atmospheric Environment*, *40*(26), 4986–4998. https://doi.org/10.1016/j.atmosenv.2005.12.066

Goldberg, D. L., Loughner, C. P., Tzortziou, M., Stehr, J. W., Pickering, K. E., Marufu, L. T., & et al. (2014). Higher surface ozone concentrations over the Chesapeake Bay than over the adjacent land: Observations and models from the DISCOVER-AQ and CBODAQ campaigns. *Atmospheric Environment*, *84*, 9–19. https://doi.org/10.1016/j.atmosenv.2013.11.008

Guenther, A. B., Jiang, X., Heald, C. L., Sakulyanontvittaya, T., Duhl, T., Emmons, L. K., & et al. (2012). The Model of Emissions of Gases and Aerosols from Nature version 2.1 (MEGAN2.1): An extended and updated framework for modeling biogenic emissions. *Geoscientific Model Development*, *5*(6), 1471–1492. https://doi.org/10.5194/gmd-5-1471-2012

Guo, H., Sullivan, A. P., Campuzano-Jost, P., Schroder, J. C., Lopez-Hilfiker, F. D., Dibb, J. E., et al. (2016). Fine particle pH and the partitioning of nitric acid during winter in the Northeastern United States. *Journal of Geophysical Research: Atmospheres*, *121*, 10,355–10,376. https://doi.org/10.1002/2016JD025311

Gustafsson, R. J., Kyriakou, G., & Lambert, R. M. (2009). The molecular mechanism of tropospheric nitrous acid production on mineral dust surfaces. *Chemphyschem*, *9*, 1390–1393. https://doi.org/10.1002/cphc.20080025

Hand, J. L., Copeland, S. A., Day, D. E., Diller, A. M., Idresand, H., Malm, W. C., et al. (2011). IMPROVE (Interagency Monitoring of Protected Visual Environments): Spatial and seasonal patterns and temporal variability of haze and its constituents in the United States, Rep. V, Coop. Inst. For Res. In the Atmos., Fort Collins, Colo. Retrieved from http://vista.cira.colostate.edu/Improve/spatial-and-seasonal-patterns-and-temporal-variability-of-haze-and-its-constituents-in-the-united-states-report-v-june-2011/

Heald, C. L., Collett, J. L. Jr., Lee, T., Benedict, K. B., Schwandner, F. M., Li, Y., et al. (2012). Atmospheric ammonia and particulate inorganic nitrogen over the United States. *Atmospheric Chemistry and Physics*, *12*(21), 10,295–10,312. https://doi.org/10.5194/acp-12-10295-2012

Henderson, B., Simon, H., Timin, B., Dolwick, P., Owen, C., Eyth, A., et al. (2017). Evaluation of NO$_x$ emissions and modeling, Abstract A42E-04, *American Geophysical Union Fall Meeting*, 11–15 December 2017, New Orleans.

Henderson, B. H., Pinder, R. W., Crooks, J., Cohen, R. C., Carlton, A. G., Pye, H. O. T., & et al. (2012). Combining Bayesian methods and aircraft observations to constrain the HO· + NO$_2$ reaction rate. *Atmospheric Chemistry and Physics*, *12*(2), 653–667. https://doi.org/10.5194/acp-12-653-2012

Hertel, O., Skjøth, C. A., Reis, S., Bleeker, A., Harrison, R. M., Cape, J. N., et al. (2012). Governing processes for reactive nitrogen compounds in the European atmosphere. *Biogeosciences*, *9*(12), 4921–4954. https://doi.org/10.5194/bg-9-4921-2012

Hodzic, A., & Jimenez, J. L. (2011). Modeling anthropogenically controlled secondary organic aerosols in a megacity: A simplified framework for global and climate models. *Geoscientific Model Development*, *4*(4), 901–917. https://doi.org/10.5194/gmd-4-901-2011

Holmes, C. D., Prather, M. J., & Vinken, G. C. M. (2014). The climate impact of ship NO$_x$ emissions: An improved estimate accounting for plume chemistry. *Atmospheric Chemistry and Physics*, *14*(13), 6801–6812. https://doi.org/10.5194/acp-14-6801-2014

Holt, J., Selin, N. E., & Solomon, S. (2015). Changes in inorganic fine particulate matter sensitivities to precursors due to large-scale US emissions reductions. *Environmental Science & Technology*, *49*(8), 4834–4841. https://doi.org/10.1021/acs.est.5b00008

Holtslag, A. A. M., & Boville, B. A. (1993). Local versus nonlocal boundary-layer diffusion in a global climate model. *Journal of Climate*, *6*(10), 1825–1842. https://doi.org/10.1175/1520-0442(1993)006<1825:LVNBLD>2.0.CO;2

Hu, L., Millet, D. B., Baasandorj, M., Griffis, T. J., Travis, K. R., Tessum, C. W., et al. (2015). Emissions of C$_6$–C$_8$ aromatic compounds in the United States: Constraints from tall tower and aircraft measurements. *Journal of Geophysical Research: Atmospheres*, *120*, 826–842. https://doi.org/10.1002/2014JD022627

Hudman, R. C., Jacob, D. J., Turquety, S., Leibensperger, E. M., Murray, L. T. W., & S., et al. (2007). Surface and lightning sources of nitrogen oxides over the United States: Magnitudes, chemical evolution, and outflow. *Journal of Geophysical Research*, *112*, D12S05. https://doi.org/10.1029/2006JD007912

Jacob, D. J. (2000). Heterogeneous chemistry and tropospheric ozone. *Atmospheric Environment*, *34*(12–14), 2131–2159. https://doi.org/10.1016/S1352-2310(99)00462-8

Janson, R., & Granat, L. (1999). A foliar rinse study of the dry deposition of nitric acid to a coniferous forest. *Agricultural and Forest Meteorology*, *98-99*, 683–696. https://doi.org/10.1016/S0168-1923(99)00133-1

Jenkin, M. E., Cox, R. A., & Williams, D. J. (1988). Laboratory studies of the kinetics of formation of nitrous acid from the thermal reaction of nitrogen dioxide and water vapour. *Atmospheric Environment*, *22*(3), 487–498. https://doi.org/10.1016/0004-6981(88)90194-1

Jobson, B. T., & Huangfu, Y. (2016). Impact of cold climates on vehicle emissions: The cold start air toxics pulse. CESTiCC Project 101409. Retrieved from http://cem.uaf.edu/cestic/research/jobson-airtoxic.aspx

Jobson, B. T., Huangu, Y., & Vanderschelden, G. S. (2017). High time resolution measurements of VOCs from vehicle cold starts: The air toxic cold start pulse. Abstract A53B-2227 presented at the 2017 AGU Fall Meeting, New Orleans, LA, 11-15 Dec.

Johansson, C., & Granat, L. (1986). An experimental study of the dry deposition of gaseous nitric acid to snow. *Atmospheric Environment*, *20*(6), 1165–1170. https://doi.org/10.1016/0004-6981(86)90150-2

Kenagy, H. S., Sparks, T. L., Ebben, C. J., Wooldridge, P. J., Lopez-Hilker, F. D., Lee, B. H., et al. (2018). NO$_x$ lifetime and NO$_y$ partitioning during WINTER. *Journal of Geophysical Research: Atmospheres*, *123*, 9813–9827. https://doi.org/10.1029/2018JD028736

Kim, M. J., Farmer, D. K., & Bertram, T. H. (2014). Air—sea exchange of N$_2$O$_5$ and ClNO$_2$. *Proceedings of the National Academy of Sciences*, *111*(11), 3943–3948. https://doi.org/10.1073/pnas.1318694111

Kim, P. S., Jacob, D. J., Fisher, J. A., Travis, K., Yu, K., Zhu, L., et al. (2015). Sources, seasonality, and trends of southeast US aerosol: An integrated analysis of surface, aircraft, and satellite observations with the GEOS-Chem chemical transport model. *Atmospheric Chemistry and Physics*, *15*(18), 10,411–10,433. https://doi.org/10.5194/acp-15-10411-2015

Krotkov, N. A., McLinden, C. A., Li, C., Lamsal, L. N., Celarier, E. A., Marchenko, S. V., et al. (2016). Aura OMI observations of regional SO$_2$ and NO$_2$ pollution changes from 2005 to 2015. *Atmospheric Chemistry and Physics*, *16*, 4605–4629. https://doi.org/10.5194/acp-16-4605-2016

Lamarque, J.-F., Dentener, F., McConnell, J., Ro, C.-U., Shaw, M., Vet, R., et al. (2013). Multi-model mean nitrogen and sulfur deposition from the atmospheric chemistry and climate model Intercomparison project (ACCMIP): Evaluation of historical and projected future changes. *Atmospheric Chemistry and Physics*, *13*(16), 7997–8018. https://doi.org/10.5194/acp-13-7997-2013

Lamsal, L. N., Duncan, B. N., Yoshida, Y., Krotkov, N. A., Pickering, K. E., Streets, D. G., & et al. (2015). U.S. NO$_2$ trends (2005–2013): EPA air quality system (AQS) data versus improved observations from the ozone monitoring instrument (OMI). *Atmospheric Environment*, *110*, 130–143. https://doi.org/10.1016/j.atmosenv.2015.03.055

Lamsal, L. N., Martin, R. V., van Donkelaar, A., Steinbacher, M., Celarier, E. A., Bucsela, E., et al. (2008). Ground-level nitrogen dioxide concentrations inferred from the satellite-borne ozone monitoring instrument. *Journal of Geophysical Research*, *113*, D16308. https://doi.org/10.1029/2007JD009235

Lee, B. H., Lopez-Hilfiker, F. D., Mohr, C., Kurtén, T., Worsnop, D. R., & Thornton, J. A. (2014). An iodide-adduct high-resolution time-of-flight chemical-ionization mass spectrometer: Application to atmospheric inorganic and organic compounds. *Environmental Science & Technology*, *48*(11), 6309–6317. https://doi.org/10.1021/es500362a

Lee, B. H., Lopez-Hilfiker, F. D., Veres, P. R., McDuffie, E. E., Fibiger, D. L., Sparks, T. L., et al. (2018). Flight deployment of a high-resolution time-of-flight chemical ionization mass spectrometer: Observations of reactive halogen and nitrogen oxide species. *Journal of Geophysical Research: Atmospheres*, *123*, 7670–7686. https://doi.org/10.1029/2017JD028082

Lee, C., Martin, R. V., van Donkelaar, A., Lee, H., Dickerson, R. R., Hains, J. C., et al. (2011). SO_2 emissions and lifetimes: Estimates from inverse modeling using in situ and global, space-based (SCIAMACHY and OMI) observations. *Journal of Geophysical Research*, *116*, D06304. https://doi.org/10.1029/2010JD014758

Lewis, J. R., Welton, E. J., Molod, A. M., & Joseph, E. (2013). Improved boundary layer depth retrievals from MPLNET. *Journal of Geophysical Research: Atmospheres*, *118*, 9870–9879. https://doi.org/10.1002/jgrd.50570

Li, Q., Zhang, L., Wang, T., Tham, Y. J., Ahmadov, R., Xue, L., et al. (2016). Impacts of heterogeneous uptake of dinitrogen pentoxide and chlorine activation on ozone and reactive nitrogen partitioning: Improvement and application of the WRF-Chem model in southern China. *Atmospheric Chemistry and Physics*, *16*(23), 14,875–14,890. https://doi.org/10.5194/acp-16-14875-2016

Li, Q. B., Jacob, D. J., Yantosca, R. M., Munger, J. W., & Parrish, D. D. (2004). Export of NO_y from the North American boundary layer: Reconciling aircraft observations and global model budgets. *Journal of Geophysical Research*, *109*, D02313. https://doi.org/10.1029/2003JD004086

Liang, J., Horowitz, L. W., Jacob, D. J., Wang, Y., Fiore, A. M., Logan, J. A., et al. (1998). Seasonal variations of reactive nitrogen species and ozone over the United States, and export fluxes to the global atmosphere. *Journal of Geophysical Research*, *103*(D11), 13435–13450. https://doi.org/10.1029/97JD03126

Lin, J.-T., & McElroy, M. B. (2010). Impacts of boundary layer mixing on pollutant vertical profiles in the lower troposphere: Implications to satellite remote sensing. *Atmospheric Environment*, *44*(14), 1726–1739. https://doi.org/10.1016/j.atmosenv.2010.02.009

Liu, H., Jacob, D. J., Bey, I., & Yantosca, R. M. (2001). Constraints from ^{210}Pb and [7]Be on wet deposition and transport in a global three-dimensional chemical. *Journal of Geophysical Research*, *106*(D11), 12,109–12,128. https://doi.org/10.1029/2000JD900839

Lu, Z., Streets, D. G., de Foy, B., Lamsal, L. N., Duncan, B. N., & Xing, J. (2015). Emissions of nitrogen oxides from US urban areas: Estimation from ozone monitoring instrument retrievals for 2005–2014. *Atmospheric Chemistry and Physics*, *15*(18), 10,367–10,383. https://doi.org/10.5194/acp-15-10367-2015

Lucchesi, R. (2013). File specification for GEOS-5 FP. GMAO office note no. 4 (version 1.0), (63 pp.). Retrieved from http://gmao.gsfc.nasa.gov/pubs/office_notes.

Luecken, D. J., Hutzell, W. T., Strum, M. L., & Pouliot, G. A. (2012). Regional sources of atmospheric formaldehyde and acetaldehyde, and implication for atmospheric modeling. *Atmospheric Environment*, *47*, 477–490. https://doi.org/10.1016/j.atmosenv.2011.10.005

Macintyre, H. L., & Evans, M. J. (2010). Sensitivity of a global model to the uptake of N_2O_5 by tropospheric aerosol. *Atmospheric Chemistry and Physics*, *10*, 7409–7414. https://doi.org/10.5194/acp-10-7409-2010

Mak, J., Gross, S., & Bertram, A. K. (2007). Uptake of NO_3 on soot and pyrene surfaces. *Geophysical Research Letters*, *34*, L10804. https://doi.org/10.1029/2007GL029756

Mao, J., Jacob, D. J., Evans, M. J., Olson, J. R., Ren, X., Brune, W. H., et al. (2010). Chemistry of hydrogen oxide radicals (HO_x) in the Arctic troposphere in spring. *Atmospheric Chemistry and Physics*, *10*(13), 5823–5838. https://doi.org/10.5194/acp-10-5823-2010

Mao, J., Paulot, F., Jacob, D. J., Cohen, R. C., Crounse, J. D., Wennberg, P. O., et al. (2013). Ozone and organic nitrates over the eastern United States: Sensitivity to isoprene chemistry. *Journal of Geophysical Research: Atmospheres*, *118*, 11,256–11,268. https://doi.org/10.1002/jgrd.50817

Martin, R. V., Jacob, D. J., Chance, K., Kurosu, T. P., Palmer, P. I., & Evans, M. J. (2003). Global inventory of nitrogen oxide emissions constrained by space-based observations of NO_2 columns. *Journal of Geophysical Research*, *108*(D17), 4537. https://doi.org/10.1029/2003JD003453

McDonald, B. C., Dallmann, T. R., Martin, E. W., & Harley, R. A. (2012). Long-term trends in nitrogen oxide emissions from motor vehicles at national, state, and air basin scales. *Journal of Geophysical Research*, *117*, D00V18. https://doi.org/10.1029/2012JD018304

McDuffie, E. E., Fibiger, D. L., Dubé, W. P., Lopez-Hilfiker, F., Lee, B. H., Thornton, J. A., et al. (2018). Heterogeneous N_2O_5 uptake during WINTER: Aircraft measurements during the 2015 WINTER campaign and critical evaluation of current parameterizations. *Journal of Geophysical Research: Atmospheres*, *123*, 4345–4372. https://doi.org/10.1002/2018JD028336

Mielke, L. H., Furgeson, A., & Osthoff, H. D. (2011). Observation of $ClNO_2$ in a mid-continental urban environment. *Environmental Science & Technology*, *45*(20), 8889–8896. https://doi.org/10.1021/es201955u

Mollner, A. K., Valluvadasan, S., Feng, L., Sprague, M. K., Okumura, M., Milligan, D. B., et al. (2010). Rate of gas phase association of hydroxyl radical and nitrogen dioxide. *Science*, *330*(6004), 646–649. https://doi.org/10.1126/science.1193030

Monks, S. A., Arnold, S. R., Emmons, L. K., Law, K. S., Turquety, S., Duncan, B. N., et al. (2015). Multi-model study of chemical and physical controls on transport of anthropogenic and biomass burning pollution to the Arctic. *Atmospheric Chemistry and Physics*, *15*(6), 3575–3603. https://doi.org/10.5194/acp-15-3575-2015

Munger, J. W., Wofsy, S. C., Bakwin, P. S., Fan, S.-M., Goulden, M. L., Daube, B. C., et al. (1996). Atmospheric deposition of reactive nitrogen oxides and ozone in a temperate deciduous forest and a subarctic woodland: 1. Measurements and mechanisms. *Journal of Geophysical Research*, *101*(D7), 12,639–12,657. https://doi.org/10.1029/96JD00230

Naik, V., Voulgarakis, A., Fiore, A. M., Horowitz, L. W., Lamarque, J.-F., Lin, M., et al. (2013). Preindustrial to present-day changes in tropospheric hydroxyl radical and methane lifetime from the Atmospheric Chemistry and Climate Model Intercomparison Project (ACCMIP). *Atmospheric Chemistry and Physics*, *13*(10), 5277–5298. https://doi.org/10.5194/acp-13-5277-2013

Osthoff, H. D., Roberts, J. M., Ravishankara, A. R., Williams, E. J., Lerner, B. M., Sommariva, R., et al. (2008). High levels of nitryl chloride in the polluted subtropical marine boundary layer. *Nature Geoscience*, *1*(5), 324–328. https://doi.org/10.1038/ngeo177

Parrish, D. D., Ryerson, T. B., Holloway, J. S., Neuman, J. A., Roberts, J. M., Williams, J., et al. (2004). Fraction and composition of NO_y transported in air masses lofted from the North American continental boundary layer. *Journal of Geophysical Research*, *109*, D09302. https://doi.org/10.1029/2003JD004226

Phillips, G. J., Thieser, J., Tang, M., Sobanski, N., Schuster, G., Fachinger, J., et al. (2016). Estimating N_2O_5 uptake coefficients using ambient measurements of NO_3, N_2O_5, $ClNO_2$ and particle-phase nitrate. *Atmospheric Chemistry and Physics*, *16*(20), 13,231–13,249. https://doi.org/10.5194/acp-16-13231-2016

Pryor, S. C., Barthelmie, R. J., Jensen, B., Jensen, N. O., & Sørensen, L. L. (2002). HNO_3 fluxes to a deciduous forest derived using gradient and REA methods. *Atmospheric Environment*, *36*(39-40), 5993–5999. https://doi.org/10.1016/S1352-2310(02)00765-3

Pye, H. O. T., Liao, H., Wu, S., Mickley, L. J., Jacob, D. J., Henze, D. K., & et al. (2009). Effect of changes in climate and emissions on future sulfate-nitrate-ammonium aerosol levels in the United States. *Journal of Geophysical Research*, *114*, D01205. https://doi.org/10.1029/2008JD010701

Pye, H. O. T., Zuend, A., Fry, J. L., Isaacman-VanWertz, G., Capps, S. L., Appel, K. W., et al. (2018). Coupling of organic and inorganic aerosol systems and the effect on gas–particle partitioning in the southeastern US. *Atmospheric Chemistry and Physics*, *18*(1), 357–370. https://doi.org/10.5194/acp-18-357-2018

Ramazan, K. A., Syomin, D., & Finlayson-Pitts, B. J. (2004). The photochemical production of HONO during the heterogeneous hydrolysis of NO_2. *Physical Chemistry Chemical Physics*, *6*(14), 3836–3843. https://doi.org/10.1039/b402195a

Riedel, T. P., Wolfe, G. M., Danas, K. T., Gilman, J. B., Kuster, W. C., Bon, D. M., et al. (2014). An MCM modeling study of nitryl chloride ($ClNO_2$) impacts on oxidation, ozone production and nitrogen oxide partitioning in polluted continental outflow. *Atmospheric Chemistry and Physics*, *14*(8), 3789–3800. https://doi.org/10.5194/acp-14-3789-2014

Russell, A. R., Valin, L. C., & Cohen, R. C. (2012). Trends in OMI NO_2 observations over the United States: Effects of emission control technology and the economic recession. *Atmospheric Chemistry and Physics*, *12*(24), 12,197–12,209. https://doi.org/10.5194/acp-12-12197-2012

Salmon, O. E., Shepson, P. B., Ren, X., He, H., Hall, D. L., Dickerson, D. D., et al. (2018). Top-down estimates of NO_x and CO emissions from Washington, D.C.-Baltimore during the WINTER campaign. *Journal of Geophysical Research: Atmospheres*, *123*, 7705–7724. https://doi.org/10.1029/2018JD028539

Sander, S., Friedl, R., Abbatt, J., Barker, J., Golden, D., Kolb, C., et al. (2011). Chemical kinetics and photochemical data for use in atmospheric studies. *JPL Publication*, *17*, 10–16.

Sarwar, G., Simon, H., Bhave, P., & Yarwood, G. (2012). Examining the impact of heterogeneous nitryl chloride production on air quality across the United States. *Atmospheric Chemistry and Physics*, *12*(14), 6455–6473. https://doi.org/10.5194/acp-12-6455-2012

Sarwar, G., Simon, H., Xing, J., & Mathur, R. (2014). Importance of tropospheric $ClNO_2$ chemistry across the Northern Hemisphere. *Geophysical Research Letters*, *41*, 4050–4058. https://doi.org/10.1002/2014GL059962

Schroder, J. C., Campuzano-Jost, P., Day, D. A., Shah, V., Larson, K., Sommers, J. M., et al. (2018). Sources and secondary production of organic aerosols in the Northeastern US during winter. *Journal of Geophysical Research: Atmospheres*, *123*, 7771–7796. https://doi.org/10.1029/2018JD028475

Seinfeld, J. H., & Pandis, S. N. (2006). *Atmospheric chemistry and physics: From air pollution to climate change* (3rd ed.). Hoboken, NJ: John Wiley.

Shah, V., Jaeglé, L., Thornton, J. A., Lopez-Hilfiker, F. D., Lee, B. H., Schroder, J. C., et al. (2018). Chemical feedbacks weaken the wintertime response of particulate sulfate and nitrate to emissions reductions over the eastern U.S. *Proceedings of the National Academy of Sciences*, *115*(32), 8110–8115. https://doi.org/10.1073/pnas.1803295115

Shindell, D. T., Faluvegi, G., Stevenson, D. S., Krol, M. C., Emmons, L. K., Lamarque, J.-F., et al. (2006). Multimodel simulations of carbon monoxide: Comparison with observations and projected near-future changes. *Journal of Geophysical Research*, *111*, D19306. https://doi.org/10.1029/2006JD007100

Shiraiwa, M., Li, Y., Tsimpidi, A. P., Karydis, V. A., Berkemeier, T., Pandis, S. N., et al. (2017). Global distribution of particle phase state in atmospheric secondary organic aerosol. *Nature Communications*, *8*, 15002. https://doi.org/10.1038/ncomms15002

Sievering, H., Kelly, T., McConville, G., Seibold, C., & Turnipseed, A. (2001). Nitric acid dry deposition to conifer forests: Niwot ridge spruce-fir-pine study. *Atmospheric Environment*, *35*(22), 3851–3859. https://doi.org/10.1016/S1352-2310(01)00156-X

Simon, H., Baker, K. R., & Phillips, S. (2012). Compilation and interpretation of photochemical model performance statistics published between 2006 and 2012. *Atmospheric Environment*, *61*, 124–139. https://doi.org/10.1016/j.atmosenv.2012.07.012

Simpson, D., Andersson, C., Christensen, J. H., Engardt, M., Geels, C., Nyiri, A., et al. (2014). Impacts of climate and emission changes on nitrogen deposition in Europe: A multi-model study. *Atmospheric Chemistry and Physics*, *14*(13), 6995–7017. https://doi.org/10.5194/acp-14-6995-2014

Snow, J. A., Heikes, B. G., Merrill, J. T., Wimmers, A. J., Moody, J. L., & Cantrell, C. A. (2003). Winter-spring evolution and variability of HO_x reservoir species, hydrogen peroxide, and methyl hydroperoxide, in the northern middle to high latitudes. *Journal of Geophysical Research*, *108*(D4), 8362. https://doi.org/10.1029/2002JD002172

Song, M., Liu, P. F., Hanna, S. J., Zaveri, R. A., Potter, K., You, Y., et al. (2016). Relative humidity-dependent viscosity of secondary organic material from toluene photo-oxidation and possible implications for organic particulate matter over megacities. *Atmospheric Chemistry and Physics*, *16*(14), 8817–8830. https://doi.org/10.5194/acp-16-8817-2016

Souri, A. H., Choi, Y., Jeon, W., Li, X., Pan, S., Diao, L., & et al. (2016). Constraining NO_x emissions using satellite NO_2 measurements during 2013 DISCOVER-AQ Texas campaign. *Atmospheric Environment*, *131*, 371–381. https://doi.org/10.1016/j.atmosenv.2016.02.020

Spataro, F., & Ianniello, A. (2014). Sources of atmospheric nitrous acid: State of the science, current research needs, and future prospects. *Journal of the Air & Waste Management Association*, *64*(11), 1232–1250. https://doi.org/10.1080/10962247.2014.952846

Steinbacher, M., Zellweger, C., Schwarzenbach, B., Bugmann, S., Buchmann, B., Ordonez, C., et al. (2007). Nitrogen oxides measurements at rural sites in Switzerland: Bias of conventional measurement techniques. *Journal of Geophysical Research*, *112*, D11307. https://doi.org/10.1029/2006JD007971

Strode, S. A., Duncan, B. N., Yegorova, E. A., Kouatchou, J., Ziemke, J. R., & Douglass, A. R. (2015). Implications of carbon monoxide bias for methane lifetime and atmospheric composition in chemistry climate models. *Atmospheric Chemistry and Physics*, *15*(20), 11789–11805. https://doi.org/10.5194/acp-15-11789-2015

Thornton, J. A., Braban, C. F., & Abbatt, J. P. D. (2003). N_2O_5 hydrolysis on sub-micron organic aerosol: The effect of relative humidity, particle phase and particle size. *Physical Chemistry Chemical Physics*, *5*(20), 4593–4603. https://doi.org/10.1039/B307498F

Thornton, J. A., Kercher, J. P., Riedel, T. P., Wagner, N. L., Cozic, J., Holloway, J. S., et al. (2010). A large atomic chlorine source inferred from mid-continental reactive nitrogen chemistry. *Nature*, *464*(7286), 271–274. https://doi.org/10.1038/nature08905

Tie, X., Brasseur, G., Emmons, L., Horowitz, L., & Kinnison, D. (2001). Effects of aerosols on tropospheric oxidants: A global model study. *Journal of Geophysical Research*, *106*(D19), 22,931–22,964. https://doi.org/10.1029/2001JD900206

Tong, D. Q., Lamsal, L., Pan, L., Ding, C., Kim, H., Lee, P., et al. (2015). Long-term NO_x trends over large cities in the United States during the great recession: Comparison of satellite retrievals, ground observations, and emission inventories. *Atmospheric Environment*, *107*, 70–84. https://doi.org/10.1016/j.atmosenv.2015.01.035

Travis, K. R., Jacob, D. J., Fisher, J. A., Kim, P. S., Marais, E. A., Zhu, L., et al. (2016). Why do models overestimate surface ozone in the Southeast United States? *Atmospheric Chemistry and Physics*, *16*(21), 13,561–13,577. https://doi.org/10.5194/acp-16-13561-2016

Valdez, M. P., Bales, R. C., Stanley, D. A., & Dawson, G. A. (1987). Gaseous deposition to snow: 1. Experimental study of SO_2 and NO_2 deposition. *Journal of Geophysical Research*, *92*(D8), 9779–9787. https://doi.org/10.1029/JD092iD08p09779

van der Werf, G. R., Randerson, J. T., Giglio, L., van Leeuwen, T. T., Chen, Y., Rogers, B. M., et al. (2017). Global fire emissions estimates during 1997–2016. *Earth System Science Data*, *9*(2), 697–720. https://doi.org/10.5194/essd-9-697-2017

VanderSchelden, G., de Foy, B., Herring, C., Kaspari, S., VanReken, T., & Jobson, B. (2017). Contributions of wood smoke and vehicle emissions to ambient concentrations of volatile organic compounds and particulate matter during the Yakima wintertime nitrate study. *Journal of Geophysical Research: Atmospheres*, *122*, 1871–1883. https://doi.org/10.1002/2016JD025332

Vasilakos, P., Russell, A., Weber, R., & Nenes, A. (2018). Understanding nitrate formation in a world with less sulfate. *Atmospheric Chemistry and Physics*, *18*, 12,765–12,775. https://doi.org/10.5194/acp-18-12765-2018

Vinken, G. C. M., Boersma, K. F., Jacob, D. J., & Meijer, E. W. (2011). Accounting for non-linear chemistry of ship plumes in the GEOS-Chem global chemistry transport model. *Atmospheric Chemistry and Physics*, *11*(22), 11,707–11,722. https://doi.org/10.5194/acp-11-11707-2011

Walker, J. M., Philip, S., Martin, R. V., & Seinfeld, J. H. (2012). Simulation of nitrate, sulfate, and ammonium aerosols over the United States. *Atmospheric Chemistry and Physics*, *12*(22), 11,213–11,227. https://doi.org/10.5194/acp-12-11213-2012

Wallace, H. W., Jobson, B. T., Erickson, M. H., McCoskey, J. K., VanReken, T. M., Lamb, B. K., et al. (2012). Comparison of wintertime CO to NOx ratios to MOVES and MOBILE6.2 on-road emissions inventories. *Atmospheric Environment*, *63*, 289–297. https://doi.org/10.1016/j.atmosenv.2012.08.062

Wang, C., Corbett, J. J., & Firestone, J. (2008). Improving spatial representation of global ship emissions inventories. *Environmental Science & Technology*, *42*(1), 193–199. https://doi.org/10.1021/es0700799

Wang, Q., Jacob, D. J., Fisher, J. A., Mao, J., Leibensperger, E. M., Carouge, C. C., et al. (2011). Sources of carbonaceous aerosols and deposited black carbon in the Arctic in winter-spring: Implications for radiative forcing. *Atmospheric Chemistry and Physics*, *11*(23), 12,453–12,473. https://doi.org/10.5194/acp-11-12453-2011

Wang, X., Wang, H., Xue, L., Wang, T., Wang, L., Gu, R., et al. (2017). Observations of N_2O_5 and $ClNO_2$ at a polluted urban surface site in North China: High N_2O_5 uptake coefficients and low $ClNO_2$ product yields. *Atmospheric Environment*, *156*, 125–134. https://doi.org/10.1016/j.atmosenv.2017.02.035

Wang, Y., Jacob, D. J., & Logan, J. A. (1998). Global simulation of tropospheric O_3-NO_x-hydrocarbon chemistry: 1. Model formulation. *Journal of Geophysical Research*, *109*(D22), 10,713–10,725. https://doi.org/10.1029/98JD00158

Washenfelder, R. A., Wagner, N. L., Dube, W. P., & Brown, S. S. (2011). Measurement of atmospheric ozone by cavity ring-down spectroscopy. *Environmental Science & Technology*, *45*(7), 2938–2944. https://doi.org/10.1021/es103340u

Weinheimer, A. J., Walega, J. G., Ridley, B. A., Gary, B. L., Blake, D. R., Blake, N. J., et al. (1994). Meridional distributions of NO_x, NO_y, and other species in the lower stratosphere and upper troposphere during AASE II. *Geophysical Research Letters*, *21*(23), 2583–2586. https://doi.org/10.1029/94GL01897

Wesely, M. (1989). Parameterization of surface resistances to gaseous dry deposition in regional-scale numerical models. *Atmospheric Environment*, *23*(6), 1293–1304. https://doi.org/10.1016/0004-6981(89)90153-4

Wesely, M., & Hicks, B. (2000). A review of the current status of knowledge on dry deposition. *Atmospheric Environment*, *34*(12-14), 2261–2282. https://doi.org/10.1016/S1352-2310(99)00467-7

Wexler, A. S., & Clegg, S. L. (2002). Atmospheric aerosol models for systems including the ions H^+, NH_4^+, Na^+, SO_4^{2-}, NO_3^-, Cl^-, Br^-, and H_2O. *Journal of Geophysical Research*, *107*(D14), 164. https://doi.org/10.1029/2001JD000451

Wild, R. J., Edwards, P. M., Dube, W. P., Baumann, K., Edgerton, E. S., Quinn, P. K., et al. (2014). A measurement of total reactive nitrogen, NO_y, together with NO_2, NO, and O_3 via cavity ring-down spectroscopy. *Environmental Science & Technology*, *48*(16), 9609–9615. https://doi.org/10.1021/es501896w

Wooldridge, P. J., Perring, A. E., Bertram, T. H., Flocke, F. M., Roberts, J. M., Singh, H. B., et al. (2010). Total peroxy nitrates (ΣPNs) in the atmosphere: The thermal dissociation-laser induced fluorescence (TD-LIF) technique and comparisons to speciated PAN measurements. *Atmospheric Measurement Techniques*, *3*(3), 593–607. https://doi.org/10.5194/amt-3-593-2010

Yu, K., Jacob, D. J., Fisher, J. A., Kim, P. S., Marais, E. A., Miller, C. C., et al. (2016). Sensitivity to grid resolution in the ability of a chemical transport model to simulate observed oxidant chemistry under high-isoprene conditions. *Atmospheric Chemistry and Physics*, *16*(7), 4369–4378. https://doi.org/10.5194/acp-16-4369-2016

Zhang, L., Brook, J. R., & Vet, R. (2003). A revised parameterization for gaseous dry deposition in air-quality models. *Atmospheric Chemistry and Physics*, *3*(6), 2067–2082. https://doi.org/10.5194/acp-3-2067-2003

Zhang, L., Jacob, D. J., Knipping, E. M., Kumar, N., Munger, J. W., Carouge, C. C., et al. (2012). Nitrogen deposition to the United States: Distribution, sources and processes. *Atmospheric Chemistry and Physics*, *12*(10), 4539–4554. https://doi.org/10.5194/acp-12-4539-2012

Zhang, Q., Jimenez, J. L., Canagaratna, M. R., Allan, J. D., Coe, H., Ulbrich, I., et al. (2007). Ubiquity and dominance of oxygenated species in organic aerosols in anthropogenically-influenced Northern Hemisphere midlatitudes. *Geophysical Research Letters*, *34*, L13801. https://doi.org/10.1029/2007GL029979

Zhu, L., Jacob, D. J., Keutsch, F. N., Mickley, L. J., Scheffe, R., Strum, M., et al. (2017). Formaldehyde (HCHO) as a hazardous air pollutant: Mapping surface air concentrations from satellite and inferring cancer risks in the United States. *Environmental Science & Technology*, *51*(10), 5650–5657. https://doi.org/10.1021/acs.est.7b01356

Zimmermann, F., Plessow, K., Queck, R., Bernhofer, C., & Matschullat, J. (2006). Atmospheric N-and S-fluxes to a spruce forest—Comparison of inferential modelling and the throughfall method. *Atmospheric Environment*, *40*(25), 4782–4796. https://doi.org/10.1016/j.atmosenv.2006.03.056